Louisiana Water Resources Research Institute
Annual Technical Report
FY 2017

Introduction

This report presents a description of the activities of the Louisiana Water Resources Research Institute for the period of March 1, 2017 to February 28, 2018 under the direction of Dr. Frank Tsai. The Louisiana Water Resources Research Institute (LWRRI) is unique among academic research institutions in the state because it is federally mandated to perform a statewide function of promoting research, education and services in water resources. The federal mandate recognizes the ubiquitous involvement of water in environmental and societal issues, and the need for a focal point for coordination.

As a member of the National Institutes of Water Resources, LWRRI is one of a network of 54 institutes nationwide initially authorized by Congress in 1964 and has been re-authorized through the Water Resources Research Act of 1984, as amended in 1996 by P.L. 104-147. Under the Act, the institutes are to:

"1) plan, conduct, or otherwise arrange for competent research that fosters, (A) the entry of new research scientists into water resources fields, (B) the training and education of future water scientists, engineers, and technicians, (C) the preliminary exploration of new ideas that address water problems or expand understanding of water and water-related phenomena, and (D) the dissemination of research results to water managers and the public.

2) cooperate closely with other colleges and universities in the State that have demonstrated capabilities for research, information dissemination and graduate training in order to develop a statewide program designed to resolve State and regional water and related land problems. Each institute shall also cooperate closely with other institutes and organizations in the region to increase the effectiveness of the institutes and for the purpose of promoting regional coordination."

The National Water Resources Institutes program establishes a broad mandate to pursue a comprehensive approach to water resource issues that are related to state and regional needs. Louisiana is the water state; no other state has so much of its cultural and economic life involved with water resource issues. The oil and gas industry, the chemical industry, port activities, tourism and fisheries are all dependent upon the existence of a deltaic landscape containing major rivers, extensive wetlands, numerous large shallow water bays, and large thick sequences of river sediments all adjacent to the Gulf of Mexico.

Louisiana has an abundance of water resources, and while reaping their benefits, faces complex and crucial water problems. Louisiana’s present water resources must be effectively managed, and the quality of these resources must be responsibly protected. A fundamental necessity is to assure continued availability and usability of the state's water supply for future generations. Specifically, Louisiana faces five major issues that threaten the quality of the state’s water supply, which are also subsets of the southeastern/island region priorities:

Nonpoint sources of pollution are estimated to account for approximately one-half of Louisiana's pollution. Because of the potential impact of this pollution and the need to mitigate its effects while maintaining the state's extensive agricultural base and coastal zones, continued research is needed in the area of nonpoint issues. Louisiana’s regulatory agencies are addressing non-point source problems through the development of waste load allocation models, modeling of atmospheric pollutants deposition to water bodies, and total maximum daily load (TMDL) calculations. There are serious technical issues that still require resolution to insure that progress is made in solving the non-point source problem.

Louisiana's vast wetlands make up approximately 40% of the nation's wetlands. These areas are composed of very sensitive and often delicately balanced ecosystems which make them particularly vulnerable to contamination or destruction resulting both from human activities and from natural occurrences.

Understanding these threats and finding management alternatives for the state's unique wetland resources are priority issues needing attention.

Water resources planning and management are ever-present dilemmas for Louisiana. Severe flooding of urban and residential areas periodically causes economic loss and human suffering, yet solutions to flooding problems can be problems in themselves. Water supply issues have also recently a focus of concern. Despite the abundance of resources, several aquifers have been in perennial overdraft, including the Southern Hills aquifer system, the Chicot aquifer system, Mississippi River alluvial aquifer, and Sparta aquifer. Louisiana passed its first legislation that restricts groundwater use in the past year. Water resources and environmental issues are intricately interconnected; therefore, changes in one aspect produce a corresponding responsive change in another. Further study is needed to understand these relationships.

Water quality protection, particularly of ground water resources, is an area of concern in Louisiana. Researchers are beginning to see contamination and salty water in drinking water supplies. Delineating aquifer recharge areas, understanding the impacts of industrial activities on water resources, evaluating nonpoint sources of pollution, and exploring protection alternatives are issues at the forefront.

Wastewater management has been a long-standing issue in Louisiana. The problem of wastewater management focuses primarily on rural and agricultural wastewater and the high costs for conventional types of wastewater treatment as found in the petrochemical industry.

The Institute is administratively housed in the College of Engineering and maintains working relationships with several research and teaching units at Louisiana State University. A Recent cooperative research projects have been conducted with LSU Agricultural Center and Louisiana Geological Survey.

During this reporting period, LWRRI continued its work on statewide groundwater management and saltwater intrusion issues. LWRRI has completed a groundwater model for the Mississippi River alluvial aquifer and a groundwater model for the Chicot aquifer. The LWRRI director advised state agencies, conducted ongoing research on saltwater encroachment modeling and remediation designs, organized a water symposium, and presented research results at local, regional and national meetings.

Research Program Introduction

The primary goal of the Institute is to help prepare water professionals and policy makers in the State of Louisiana to meet present and future needs for reliable information concerning national, regional, and state water resources issues. The specific objectives of the Institute are to fund the development of critical water resources technology, to foster the training of students to be water resources scientists and engineers capable of solving present and future water resources problems, to disseminate research results and findings to the general public, and to provide technical assistance to governmental and industrial personnel and the citizens of Louisiana.

The priority research areas for the Institute in FY 2017 focused on selected research themes developed in conjunction with the advisory board. These themes corresponded to the major water resource areas affecting Louisiana described in the Introduction above. Projects selected were from a range of faculty with different academic backgrounds including hydrologist, environmental engineers, water resource engineers, electrical engineering and scientists. Supporting research in these priority areas has increased the visibility of the Institute within the State.

The individual research projects are listed below.

Project 2016LA103B (Sherchan) Occurrence and Control of Naegleria fowleri in Groundwater Sources in Louisiana – Tulane University

Project 2016LA104B (Quirk) Assessing the Spatial Extent, Temporal Variability and Mechanisms of Inland Hypoxia in Louisiana Waters – LSU and A&M College

Project 2016LA105B (Paudel) Economic Impacts of Groundwater Salinity in Louisiana Agriculture – LSU AgCenter

Project 2017LA112B (Carlson) Determination of chloride, nitrate and other ion concentrations in Mississippi Alluvial Aquifer in Northeast Louisiana – Louisiana Geological Survey

Project 2017LA113B (Zhang) Effects of climate change on nitrogen and sulfur deposition to Louisiana water bodies using climate downscaling meteorology and chemical transport model – LSU and A&M College

Project 2017LA114B (Wang) Coupled chemical and hydraulic impacts of saltwater intrusion on the fate and transport of spilled chemicals in the Mississippi River – LSU and A&M College

Project 2017LA115B (Zhu) Desalination of salt water for agriculture based on a novel battery system – LSU and A&M College

These projects include one project that focuses on Climate and Hydrologic Processes (2017LA113B), one project that focuses on Engineering (2017LA115B), one project that focuses on biological sciences (2016LA103B) and five projects that focus on water quality (2016LA104B, 2016LA105B, 2017LA112B, and 2017LA114B).

Occurrence and Control of Naegleria fowleri in Groundwater Sources in Louisiana

Basic Information

Title:	Occurrence and Control of Naegleria fowleri in Groundwater Sources in Louisiana
Project Number:	2016LA103B
Start Date:	3/1/2016
End Date:	2/28/2018
Funding Source:	104B
Congressional District:	LA-02
Research Category:	Biological Sciences
Focus Categories:	Groundwater, Water Quality, Treatment
Descriptors:	None
Principal Investigators:	Samendra Sherchan, Jeffrey Wickliffe

Publication

1. Xue, J., Sherchan S., (2018) Occurrence and Control of Naegleria fowleri in groundwater sources in Louisiana (in preparation)

Problem and Research Objectives

Naegleria fowleri, also known as "the brain-eating amoeba", is a free living amoebae found naturally in hot springs and warm surface waters. *N. fowleri* can cause primary meningoencephalitis (PAM), a rare and fatal disease in children and young adults. In 2011, two people died of PAM caused by *N. fowleri* in DeSoto Parish and St. Bernard Parish, Louisiana. Both cases involved the use of a neti-pot. In 2013, there was second death in St. Bernard Parish (4-year old boy) caused by PAM and confirmed to be *N. fowleri* infection (Cope et. al., (2015). Testing conducted in 2013 by Louisiana Department of Health and Hospitals (DHH)/CDC in both St. Bernard and DeSoto found this amoeba in the treated distribution system water supply. To date, a total of 6 Louisiana's public water systems have tested positive for *N. fowleri* (Louisiana DHH; Bartrand et al., 2014). The occurrence of this protozoan pathogen *N. fowleri* in the treated water supplies in Louisiana causing three deaths is the basis of this research project. This pathogenic free-living amoeba grows in warm water and is fairly resistant to chlorine based disinfection (Miller et al., 2015). The goal of this study is to gain baseline knowledge of the occurrence and quantity of *N. fowleri* in non-disinfected small drinking water systems and individual household well water systems in Louisiana. Over 500,000 people depend on private wells for their drinking water in the State of Louisiana (Louisiana DHH). In addition, guidance for both utilities and the general public is needed to determine how to reduce exposure to this organism in groundwater sources in Louisiana.

The proposed project involves a field study to assess the occurrence and quantity of *Naegleria fowleri* in non-disinfected small drinking water systems and individual household well water systems in Louisiana. Other opportunistic pathogens including *Legionella* and *Mycobacteria* were quantified in private wells. The data collected will be analyzed to assess environmental and other water quality factors that may be associated with the occurrence of *N. fowleri* in these groundwater supplies.

Methodology

Sample collection

In total, 113 well water samples were collected from 55 private wells around Lake Pontchartrain Southeastern Louisiana (Fig. 1). For each site, two types of water samples were collected and they were pre- and post-flush water samples. The post-flush samples were collected after three minutes' flush and two-liter water samples were then collected and kept on ice. A YSI Pro2030 meter (YSI incorporated, OH, USA) was used to measure *in-situ* dissolved oxygen, temperature, salinity, specific conductivity, pH.

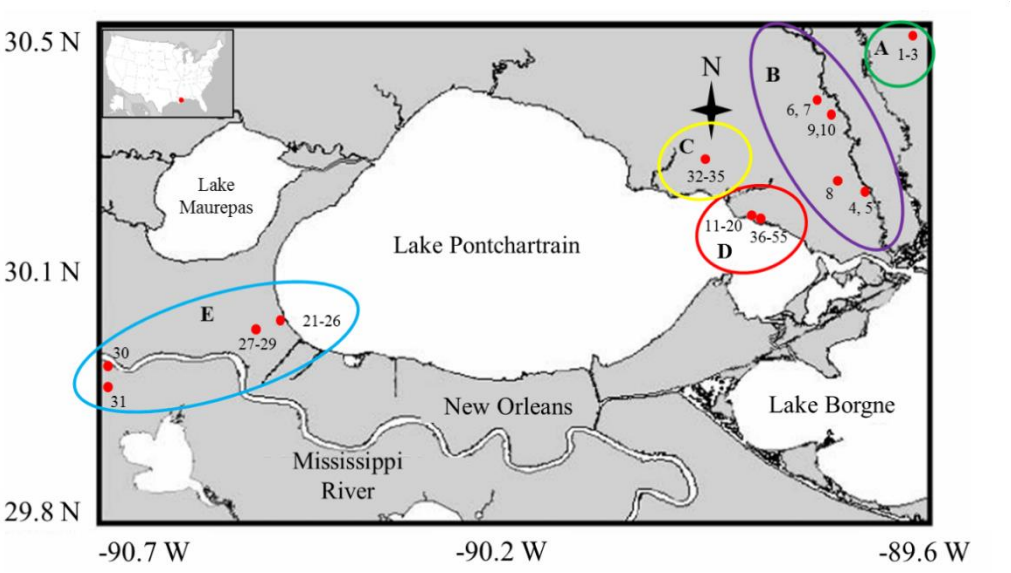

Fig.1; Private well locations around Lake Pontchartrain; The distribution of private well was divided into five sampling zones based on well location: A) Green, B) Purple, C) Yellow, D) Red, and E) Blue.

DNA extraction

On the day of sample arrival, each sample were filtered through a 0.45 µm-pore-size membrane filter (Thermo Fisher Scientific, Waltham, MA) under vacuum. After filtration, sterile forceps were used to aseptically fold each of the membrane filters and placed in separate Whirl-Pak™ bags and stored at -20°C until the DNA extraction. Genomic DNA was isolated from membrane filters using the PowerSoil DNA Isolation Kit (Mo Bio Laboratories, Inc., Carlsbad, CA) according to the manufacturer's instructions. To maximize DNA extraction efficiency, membrane filters were cut into small pieces with sterile scissors and the DNA was quantified with a NanoDrop ND-2000 UV spectrophotometer (Thermo Scientific, Wilmington, USA). The DNA samples were stored at -20°C prior to use.

Enumeration of fecal coliform, E.coli and enterococci

Fecal-indicator bacteria were measured by IDDEX method within the required time frame following sample collection. Undiluted water samples was each mixed with reagent and placed in a Quantitray/2000 according to the manufacturer's instructions (Colilert and Enterolert product insert; IDEXX Laboratories). The Colilert test kit was used for measuring total coliform bacteria and *E. coli*. An Enterolert test kit was employed for measuring enterococci (e.g. *E. faecium* and *E. faecalis*). Quantitray/2000 was sealed using Quanti-Tray Sealer and incubated at 37˚C for 24 hours (41°C for enterococci). After incubation, the wells with having a bright yellow color were quantified as positive for total coliforms for the Colilert test. The wells that fluoresced under U.V. light at 366 nm were quantified as positive for *E. coli*. For the Enterolert test, the wells that fluoresced under U.V. light at 366 nm were quantified as positive for enterococci. The number of positive wells was compared to the manufacturer-provided MPN table to enumerate fecal coliform and enterococci in terms of MPN/100 ml.

Quantitative PCR assays

Quantitative polymerase chain reaction (PCR) assays targeting *Escherichia coli (E. coli), Enterococcus, Naegleria fowleri (N. fowleri), Legionella* and *Mycobacteria* were performed using the Applied Biosystems StepOne Real-Time PCR system (Applied Biosystems, NY). Here, the reaction mixture (20 µl) contained 1x PerfeCTa qCPR ToughMix (Quanta Biosciences, Beverly, MA), 0.2 µM of each primer, and 2.5 µl of the template DNA. QPCR reactions for *N. fowleri* were performed in duplicate and amplification protocols consisted with a hold at 95°C for 3 min, followed by 45 cycles of 95°C 10s, 63°C 10 s (60°C 10 s for *E.coli*), and 72°C 10 s. QPCR reactions for *Enterococcus* were performed in duplicate and amplification protocols consisted with a hold at 95°C for 2 min, followed by 40 cycles of 95°C 15s, 60°C 60 s. Genomic DNA (*N. fowleri* ATCC 30174D; *E. coli* ATCC 700926DQ; *Legionella* ATCC; *Mycobacteria* ATCC) for each marker were used to produce calibration curve with concentrations spanning the range from 10 to 10^6 gene copies per reaction, with two replicates, was constructed. Duplicate no-template controls (NTC) were included in each run. The amplification efficiencies (AE) were calculated based on the equation: $AE= 10^{(-1/slope)}– 1$. This method detects viable organisms, including the trophozoite stage of *N. fowleri*. A summary of qPCR target organisms, primer/ probe name, and sequences are detailed in Table 1.

Table 1 Summary of qPCR assay conditions.

Target Organism	Primer or Probe Name	Sequence	References
E. coli	784F	5'-GTG TGA TAT CTA CCC GCT TCG C-3'	Frahm and Obst 2003
	866R	5'-AGA ACG GTT TGT GGT TAA TCA GGA-3'	
	Ec807	5'-FAM -TCG GCA TCC GGT CAG TGG CAG T-TAMRA-3'	
Enterococcus spp.	EnteroF1A	5'-GAG AAA TTC CAA ACG AAC TTG-3'	Ludwig and Schleifer 2000
	EnteroR1	5'-CAG TGC TCT ACC TCC ATC ATT-3'	
	Entero probe	5'-FAM-TGG TTC TCT CCG AAA TAG CTT TAG GGC TA-TAMRA-3'	
N. fowleri	NaeglF192	5'-GTG CTG AAA CCT AGC TAT TGT AAC TCA FT-3'	Qvarnstrom et al. 2006
	NaeglR344	5'-CAC TAG AAA AAG CAA ACC TGA AAG G-3'	
	NfowlP	5'- /5HEX/ATA GCA ATA/ ZEN/ TAT TCA GGG GAG CTG GGC/31ABkFQ/-3'	
Legionella	Leg23SF	5'-ACA ATC AGC CAA TTA GTA CGA GTT AGC-3'	Nazarian et al., 2008
	Leg23SR	5'-CCC ATG AAG CCC GTT GAA-3'	
	Leg23SP	5'-/56-FAM/TCC ACA CCT/ZEN/CGC CTA TCA ACG TCG TAG T/31ABkFQ/-3'	
Mycobacteria	I571-110F	5'-CCT GGG AAA CTG GGT CTA AT-3'	García-Quintanilla et al., 2002
	I571R	5'-CGC ACG CTC ACA GTT A-3'	
	Probe H19R	5'-/56-FAM/TTT CAC GAA/ZEN/CAA CGC GAC AAA CT/31ABkFQ/-3'	

Principal Findings and Significance

The chemical and physical parameters of water samples were analyzed *in situ*. The average pH value ranged between 7.3 and 10.0. The values of electrical conductivity (EC) measured varying between 334.3 and 2660.0 mS, with the highest value found in private well (PW) 29 which is located on the west shore of Lake Pontchartrain. Similarly, water salinity ranged between 0.17 and 1.31 ppt, with the highest value found in PW29. The water temperature was ranged from 17.0℃ to 39.0℃ with the highest temperature found at PW07 pre-flush. The unusual high temperature was probably because that water was collected from a water hose which lay on the ground under direct sunshine. The dissolved oxygen measured varying between 0.51 and 7.64 mg/L. Based on the information we collected from the owner of each private well, the depth of the well ranged from 200 ft to 1900 ft, with an average depth of 536 ft. The depth of PW4 and 48 was over 1000 ft.

Table 2 Analysis for chemical and physical parameters on private-well water samples

	Tm ℃	DO mg/l	pH /	EC mS	Salinity ppt	Depth of well feet
Min	17.0	0.51	7.3	334.3	0.17	200
Max	39.0	7.64	10.0	2660.0	1.31	1900
Average	25.1	3.76	8.5	753.7	0.38	536

Note: Tm indicates Temperature, DO indicate Dissolved Oxygen, EC indicates electrical conductivity.

A total of 113 water samples were analyzed by using culture method. The biological water quality of those samples was assessed by using fecal indicator bacteria (FIB) such as fecal coliform, *E. coli* and enterococci. Fecal coliform was present in 33.6% (38/113) of water samples from 20 private wells at levels ranging from 1 to 2450 CFU/100 ml. Water samples collected from PW8, 9, 10 and 30 had consistent higher counts of total coliform. Under most circumstance, the counts of fecal coliform decreased after three minutes' flushing, the decreasing rate ranged from 18.9% to 100%. The fecal coliform counts didn't change after flushing at six private wells (PW06, 21, 24, 30, 53 and 54) and the fecal coliform counts increased at three private wells (PW07, 12 and 29). *E. coli* was only detected in three water samples at value levels ranging between 1 and 2 CFU/100 ml. *E. coli* were found in Pre- and Post-flush water samples collected from PW28 which is located on the west shore of Lake Pontchartrain. The *E. coli* counts did not change after three minutes' flushing at NF28. Only 54 water samples collected from 25 wells were observed for enterococci in our research and enterococci were present in 35.2% (19/54) of water samples at levels ranging from 1 to 34.6 CFU/100 ml with the highest enterococci concentration being observed at PW24 post-flush water sample. Enterococci concentration in post flush water samples was decreased and the decreasing rates ranged from 59.5% to 100.0%, except for PW 24 and 28.

Quantitative real-time PCR were performed on private well water samples targeting *N. fowleri, E. coli, Legionella* and *Mycobacteria*. *E. coli* was detected in 43.4% (49/113) of water samples at value levels ranging from 0.53 to 3.16 Log_{10} of GC/100 ml. More samples showed positive signals with *E. coli* indicated higher sensitivity of PCR based molecular method compared with culture based method. *N. fowleri* was detected in 38.0% (43/113) of water samples, with concentration ranged from 2.10 to 4.69 Log_{10} of GC/100 ml. *Legionella* was detected in 86.7% (98/113) of water samples and *Mycobacteria* was detected in 68.1% (77/113) of water samples. QPCR results

showed most of water samples were detected positive with multiple genetic markers (Fig. 2). There were only seven water samples that were negative with all four markers.

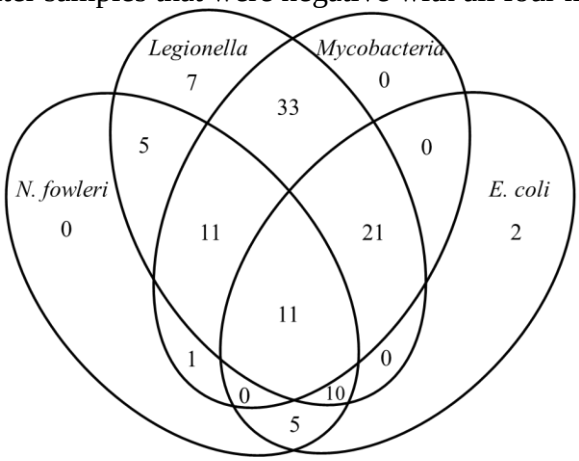

Fig. 2 *N. fowleri, Legionella, Mycobacteria,* and *E. coli* genetic markers detected in well water samples; Note: Number indicates number of samples detected positive with certain genetic markers. For samples only detected positive with single marker: *N. fowleri* (0), *Legionella* (7), *Mycobacteria* (0), and *E. coli* (2); for samples only detected positive with two of the markers: *N. fowleri* and *Legionella* (5), *Legionella* and *Mycobacteria* (33), *Mycobacteria* and *E. coli* (0), *N. fowleri* and *Mycobacteria* (1), *N. fowleri* and *E. coli* (5), *Legionella* and *E. coli* (0); for samples only detected positive with three of the markers: *N. fowleri, Legionella* and *Mycobacteria* (11), *N. fowleri, Legionella* and *E. coli* (10), *N. fowleri, Mycobacteria* and *E. coli* (0), *Legionella, Mycobacteria* and *E. coli* (21); for samples detected positive with four markers (11); for samples detected negative with all four markers (7).

Based on the private well locations, the average concentration of *E. coli* was found highest in zone D which located on the northeast shore of Lake Pontchartain (Fig. 3). None of samples from Zone A was detected positive with *E. coli*. Similar results were observed for *N. fowleri* genetic marker where none of samples from Zone A was detected positive with *N. fowleri*. The highest mean concentration was found in Zone B with average concentration of 3.3 Log_{10} of GC/100 ml. The average concentration of *Legionella* was significantly lower in Zone B and C compared with other sampling zones (Fig. 3). *Mycobacterium was* found highest in Zone E which located on the southwest shore of Lake Pontchartrain. Samples collected from Zone C and D had relatively lower concentration of *Mycobacteria* compared to other sampling zones.

A statistical significant positive correlation between well water salinity level and the concentration of *Mycobacteria* was observed ($r = 0.23$, $P < 0.05$) (Fig. 4). In addition, weak negative correlation between water salinity and *E. coli* ($r = 0.32$) and *N. fowleri* ($r = 0.13$) concentration were also observed and they were statistical significant ($P < 0.05$). The negative correlation suggesting water salinity has an adverse effect on the survival of *E. coli* and *N. fowleri* in well water. Among all genetic markers we tested, a statistical significant positive correlation between *Mycobacteria* and *Legionella* was observed ($r = 0.33$, $P < 0.05$) (Fig. 4). We also observed weak negative correlation for *N. fowleri* vs. *Mycobacteria* and *N. fowleri* vs. *Legionella*, but they were not statistically significant ($P > 0.05$). No clear relationship for *E. coli* vs. *N. fowleri* and *E. coli* vs. *Mycobacteria* was found in our study.

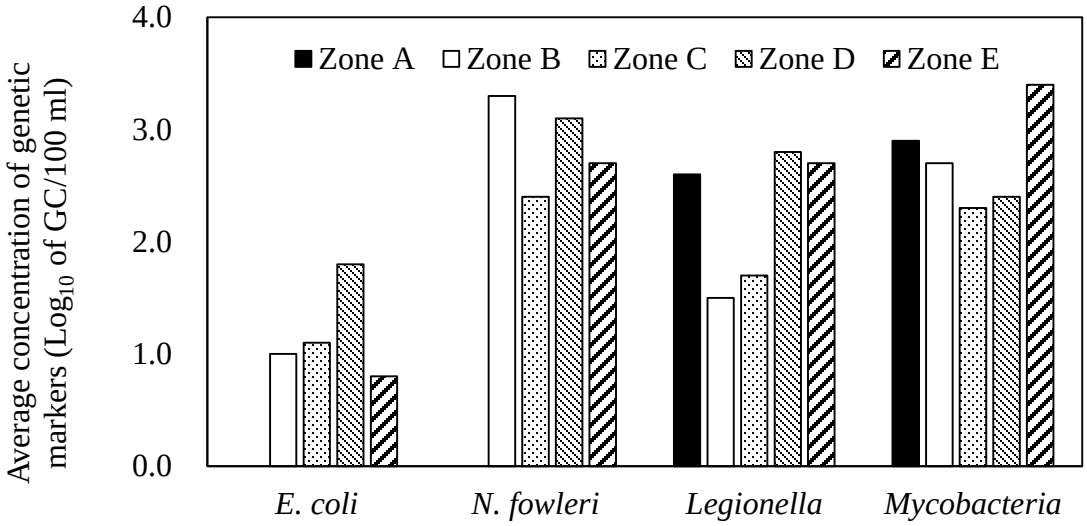

Fig. 3; the average concentration of genetic markers in well water samples collected from different sampling zone.

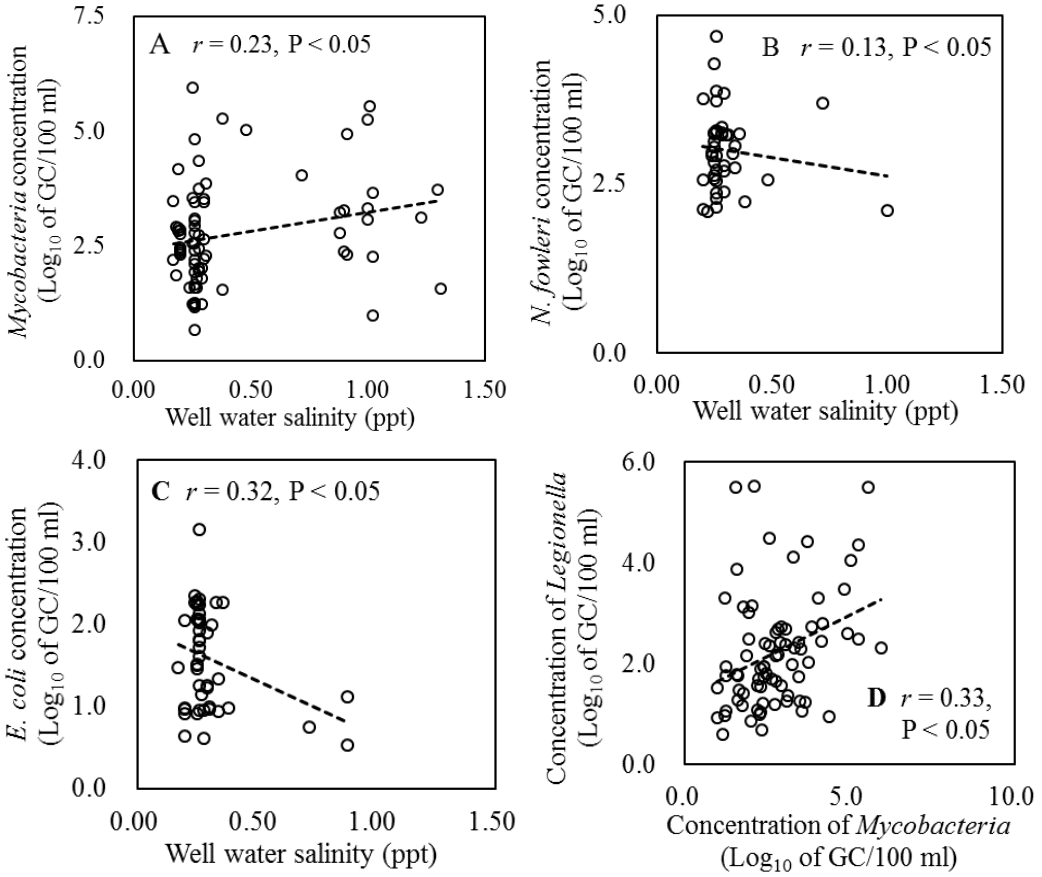

Fig. 4; Overall correlation between water salinity and (A) *Mycobacteria*, (B) *N. fowleri*, (C) *E. coli*, and (D) correlation between the concentration of *Mycobacteria and Legionel*

Assessing the Spatial Extent, Temporal Variability and Mechanisms of Inland Hypoxia in Louisiana Waters

Basic Information

Title:	Assessing the Spatial Extent, Temporal Variability and Mechanisms of Inland Hypoxia in Louisiana Waters
Project Number:	2016LA104B
Start Date:	3/1/2016
End Date:	2/28/2018
Funding Source:	104B
Congressional District:	LA-06
Research Category:	Water Quality
Focus Categories:	Water Quality, Surface Water, Nutrients
Descriptors:	None
Principal Investigators:	Tracy Quirk, Kanchan Maiti

Publications

1. Candilora, K., Quirk, T., Maiti, K. 2017. “Oxygen Dynamics in Low Flow Bayous Across Southern Louisiana” Louisiana State University, Discover Day, April 4, 2017
2. Quirk, T., Maiti, K, Candilora, K. in prep. Dissolved oxygen and oxygen consumption dynamics in low flow bayous of southeast Louisiana.
3. Candilora, K., Quirk, T., Maiti, K. 2017. “Oxygen Dynamics in Low Flow Bayous Across Southern Louisiana” Louisiana State University, Discover Day, April 4, 2017
4. Quirk, T., Maiti, K, Candilora, K. in prep. Dissolved oxygen and oxygen consumption dynamics in low flow bayous of southeast Louisiana.

Problem and Research Objectives

Streams and bayous are abundant surface water resources in south Louisiana. These streams and bayous form the link between larger rivers and lakes and coastal waters, providing water for public supply, industrial and agricultural use, and natural ecosystems. However, the quality of the water in small waterways may be impaired associated with excess nutrients, organic and inorganic substances such as heavy metals associated with surrounding land-use. Depending on whether watershed land-use is primarily agricultural or forested, both nutrient and oxygen dynamics can be altered including the timing and magnitude of low dissolved oxygen concentrations and hypoxia, where oxygen concentrations are less than 2 mg/L.

Hypoxic events in low-lying slow flowing channels may occur naturally; however, extensive river management and basin-wide land-use changes have increased their frequency and impact (Whitworth et al. 2012). In low-energy channels of the Atchafalaya River Basin, chronic hypoxic conditions are common when water temperature and river stage are high (Sabo et al. 1999). While low dissolved oxygen is common in nutrient rich shallow water when organic matter is concentrated by receding waters and biological oxygen demand is fueled by warm temperatures (Tramer 1977), Sabo et al. (1999) found chronic hypoxia in the spring and early summer when the river stage was high and phytoplankton densities and percent oxygen saturation were low. It was surmised that decomposition of organic matter and biological consumption of oxygen was causing the chronic hypoxia, although this was not tested. No relationship between low dissolved oxygen and total organic carbon was observed. Unfortunately, dissolved organic carbon (DOC) concentration was not measured and hence it cannot be determined whether microbial respiration of DOC plays an important role. For channels seasonally inundated by floodwaters, DOC is leached from plant litter, or derived from soils, living plants, algae and microorganisms (Meyer et al. 1990). The variation in sources of DOC and biological oxygen demand across low-flow streams and bayous across Louisiana is unknown. In addition, the seasonality and mechanisms of hypoxia may differ from backwater forested channels to more eutrophic channels surrounded by agriculture.

In addition to water column temperature and water levels, surrounding land-use may also play a key role in aquatic oxygen dynamics. A comparison of nutrient-poor forested and a nutrient-rich open stream in the Oria watershed in Spain illustrated strong diel fluctuations in dissolved oxygen and periodic hypoxia in the open channel, while the low nutrient forested stream experienced steady oxygen concentrations above 5 mg/L (Sabater et al. 2000). In forested systems, oxygen dynamics may be less influenced by diel changes in respiration of microorganisms decomposing algal biomass than in less light-limited open channels. Differences in oxygen dynamics may be directly related to the timing and source of nutrient and carbon input. In forested streams, much of the DOC is leached from plant litter in the form of fallen leaves (Hladyz et al. 2011). The impact on oxygen dynamics will depend on the timing and water temperature during and after litterfall. A period of leaching and physical breakdown when microbial activity is low in the fall and winter may reduce the lability of C in the spring and summer when microbial activity may be greatest. In contrast, in slow moving moderately eutrophic open bayous surrounded by agricultural land, nutrient enrichment can stimulate the growth of epiphytic and/or filamentous algae. Adverse effects of nutrient enrichment include a reduction in aeration of the water column from the loss of submerged plant photosynthesis and an increased uptake of oxygen through decomposition of surface aquatics. The water becomes hypoxic to anoxic, decomposition continues anaerobically, and plants and animals requiring oxygen cannot survive.

The objectives of this research were threefold: (1) determine the spatial extent of inland hypoxia in low-flow stream and bayous in south Louisiana in the summer; (2) examine temporal dynamics of dissolved oxygen conditions in two waterways, one with bottomland forested and the other with agricultural watershed land-use; and (3) examine possible mechanisms leading to hypoxia including biological oxygen demand, sediment organic matter content, and total and dissolved organic carbon concentrations in the two systems. Additional important co-varying parameters (e.g., temperature, pH, turbidity, flow) were also examined to inform predictive models of low oxygen conditions.

Methodology

Objective 1: *Spatial Extent of Inland Hypoxia*

To assess oxygen conditions in bayous of southeast Louisiana in the Mississippi and Atchafalaya basins, we conducted surveys of dissolved oxygen (DO), pH, temperature, conductivity, depth and width of stream, and vegetation along surveyed 8 major bayous, including the Amite River Diversion Canal, Bayou Fusil, Bayou Gross Tete, Bayou Plaquemine, Blind River, Choctaw Bayou, Old Parish Canal, and Petite Amite River (**Figure 1**). A minimum of three and up to nine random survey points approximately 1 km apart were established in each bayou. Data was collected every 50 cm from the surface to the bottom of the water column. Water column parameters were collected using an YSI Professional Plus multi-parameter probe. Instruments were calibrated prior to each sampling trip. Additional data including drainage basin size, surrounding land-use, and predominate vegetation species and form (e.g., emergent, submerged, surface) and percent cover was collected for each sample location.

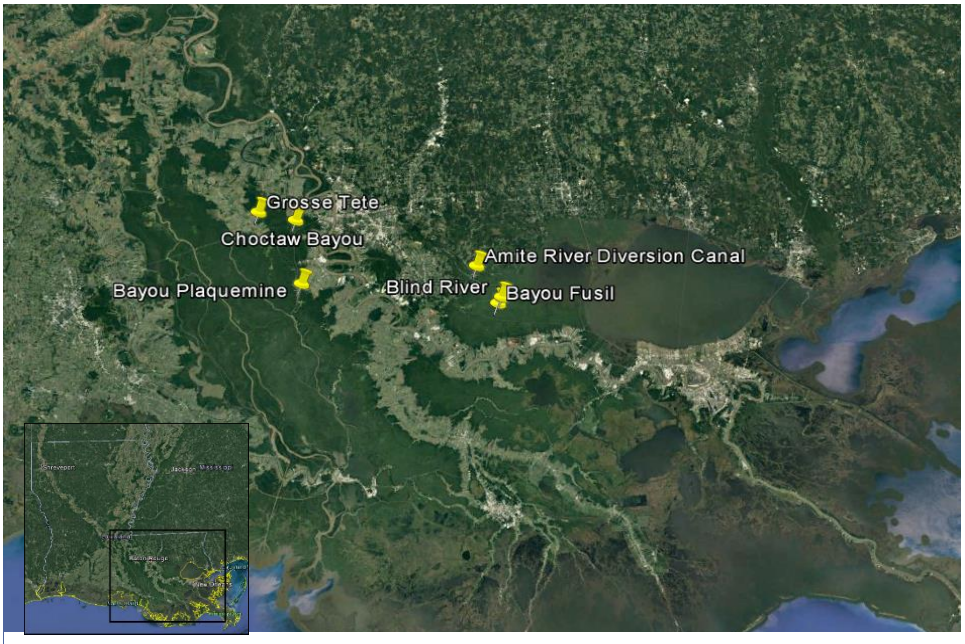

Figure 1. Survey locations in southeast Louisiana, USA.

Objective 2: *Temporal Dynamics of Dissolved Oxygen*

Based on the above survey, we selected two locations with differing watershed land-use where continuous dissolved oxygen is being monitored over a one year period. Old Parish Canal is a part of the Atchafalaya Basin and is a forested backwater bayou. The second location is in Bayou Grosse Tete, surrounded by predominantly light residential and agricultural land-use. Continuous oxygen sensors were placed approximately 10 cm above the bottom of the stream to characterize

bottom-water hypoxia over a one year period. The sensor was attached to an anchor with a corkscrew head to stabilize in the sediment.

Objective 3: *Mechanisms Leading to Hypoxic Conditions*

To examine the mechanisms involved in the formation and maintenance of hypoxic conditions in two contrasting stream types, laboratory incubations were conducted to measure biological oxygen demand and to isolate sources of carbon fueling oxygen consumption. At each of the two locations in *Objective 2*, sediment cores and water samples were collected during time periods when oxygen concentrations are less than 2 mg/L. In October 2016, we collected three sediment cores and approximately 60 L of creek water to establish three experimental units for which oxygen consumption was measured. The three units were: filtered water overlying sediment (C1), unfiltered water samples (C2) and filtered water samples (C3; **Figure 2**). Samples were incubated in air-tight core tubes or bottles at in situ temperature, and DO was recorded over time, approximately every 2 – 3 hrs until dissolved oxygen concentration dropped to zero. The oxygen consumption rates were calculated using the change in DO between sampling times. Dissolved oxygen concentration was measured using a high precision clark-type oxygen microelectrode with a detection limit of 0.05 µM (0.002 mg/L). This experiment allowed us to calculate the individual role of sediment, dissolved organic matter and suspended organic matter in consuming oxygen leading to formation of hypoxia (as per mass balance equations shown in **Figure 2**), as well as the total oxygen consumption rates at these two locations.

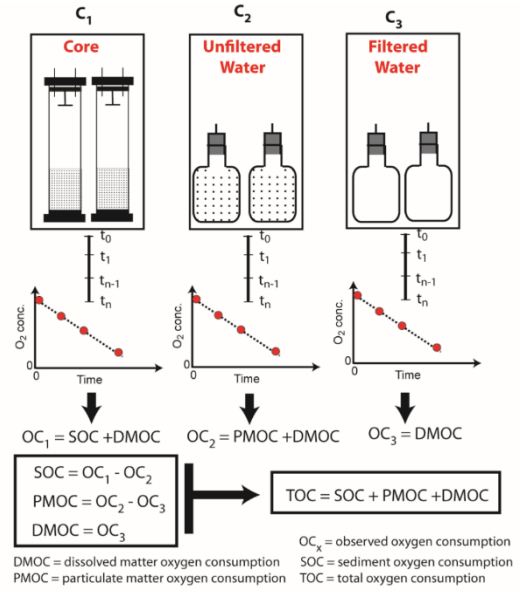

Figure 2. Schematics of oxygen consumption incubation experiment

Principal Findings and Significance

Hypoxia Survey

Seven of the eight bayous surveyed were surrounded by bottomland hardwood forest **(Table 1)**. Emergent vegetation on the sides of the stream channels ranging from an average of 6 – 29% cover of the channel area. Stream widths ranged from an average of 5 to 33 m and depths ranged from less than 1 m to an average of 4.5 m (Table 1). Temperatures were similar among bayous even when comparing streams surveyed in August to those surveyed in October, all of which averaged around 26°C. pH varied slightly and ranged from an average of 6.7 to 7.5.

Table 1. Characteristics of bayous surveyed for dissolved oxygen. Values are means ± standard errors across survey locations and depths.

			Vegetation cover (%)							
Location	Date Surveyed	Shoreline Vegetation	Emergent	Surface	Submerged	Width of Channel (m)	Depth of Channel (m)	Temp ©	Cond (uS/cm)	pH
Amite River Diversion Canal	9/16/2016	BHW	17 ± 4	16 ± 4	2.6 ± 0.8	18 ± 2	2.5 ± 0.2	27.64 ± 0.03	98.3 ± 0.2	7.0 ± 0.1
Bayou Fusil	10/2/2016	BHW	28 ± 4	0	0	14 ± 1	1.7 ± 0.1	25.28 ± 0.27	169.2 ± 2.6	7.1 ± 0.1
Bayou Gross Tete	9/9/2016	Forested/residential	29 ± 3	0	0	19 ± 1	4.0 ± 0.1	26.72 ± 0.05	140.7 ± 3.2	6.8 ± 0.1
Bayou Plaquemine	8/24/2016	BHW	7 ± 2	0	0	31 ± 2	3.0 ± 0.1	26.51 ± 0.05	76.7 ± 1.7	6.7 ± 0.1
Blind River	10/2/2016	BHW	24 ± 3	0	0	33 ± 3	4.5 ± 0.5	26.61 ± 0.12	156.2 ± 0.3	6.9 ± 0.1
Choctaw Bayou	9/18/2016	BHW	6 ± 1	0	0	14 ± 1	0.9 ± 0.1	26.66 ± 0.91	230.0 ± 28.9	7.5 ± 0.1
Old Parish Canal	9/18/2016	BHW	10 ± 0	0	0	5 ± 1	1.4 ± 0.1	27.43 ± 0.03	227.1 ± 1.8	7.5 ± 0.1
Petite Amite River	9/16/2016	BHW	9 ± 1	3 ± 1	0	21 ± 1	3.7 ± 0.2	27.90 ± 0.03	101.9 ± 0.8	6.8 ± 0.1

Oxygen concentrations ranged from 0.1 to 5.2 mg/L at the surface (**Figure 3**). Bayous with relatively high surface DO had DO concentration that declined with depth, all to below hypoxic conditions below 1.5 m depth. Bayous with low DO at the surface tended to have a relatively constant low DO with increasing depth.

The two bayous with surface oxygen concentrations above 3 mg/L were surveyed in October and thus seasonal changes may have influenced the difference between those bayous and the others in the survey. Continuous oxygen measurements will shed light on temporal changes in near-bottom oxygen concentration.

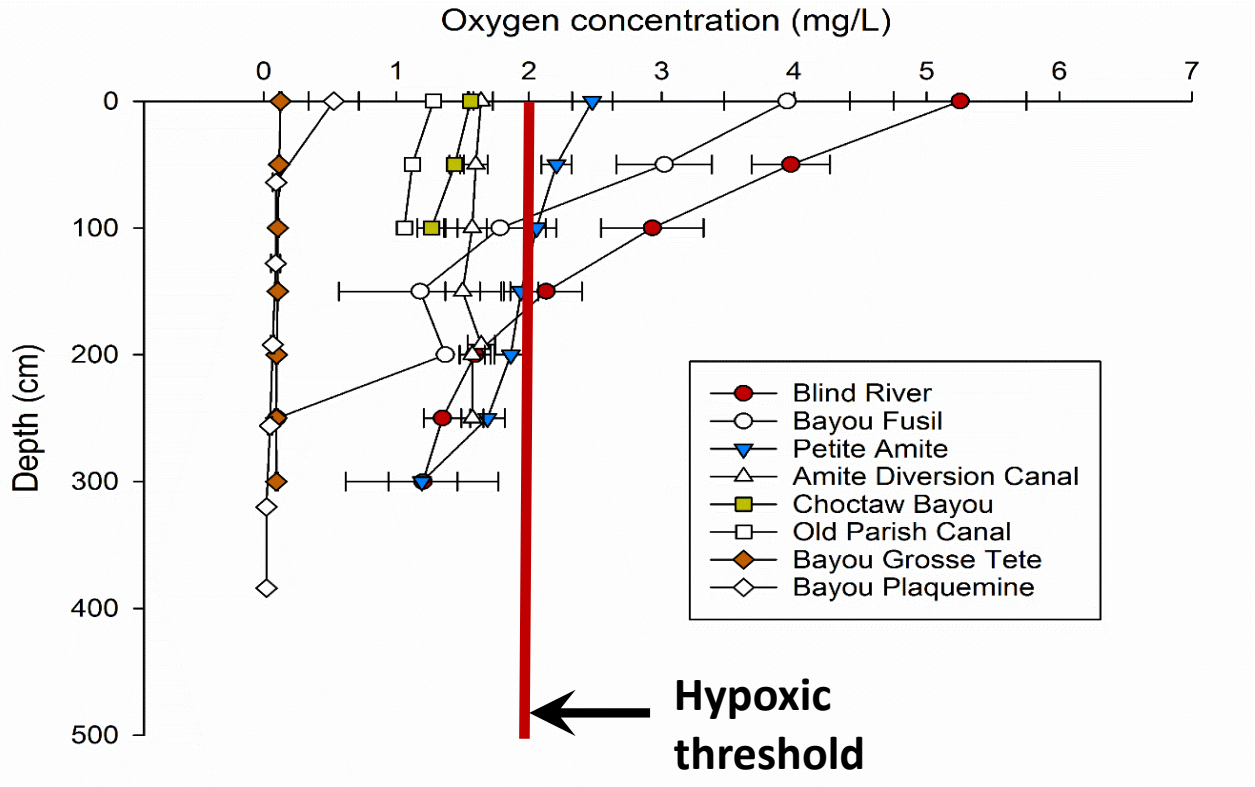

Figure 3. Dissolved oxygen concentrations in bayous of southern Louisiana August – October 2016.

Temporal Dynamics of Dissolved Oxygen

Diurnal fluctuations in DO associated with photosynthesis + respiration during the day and respiration only at night, as well as seasonal fluctuations related to temperature and biological activity are expected. The DO sensor was only recovered from GT Bayou **(Figure 4)**.

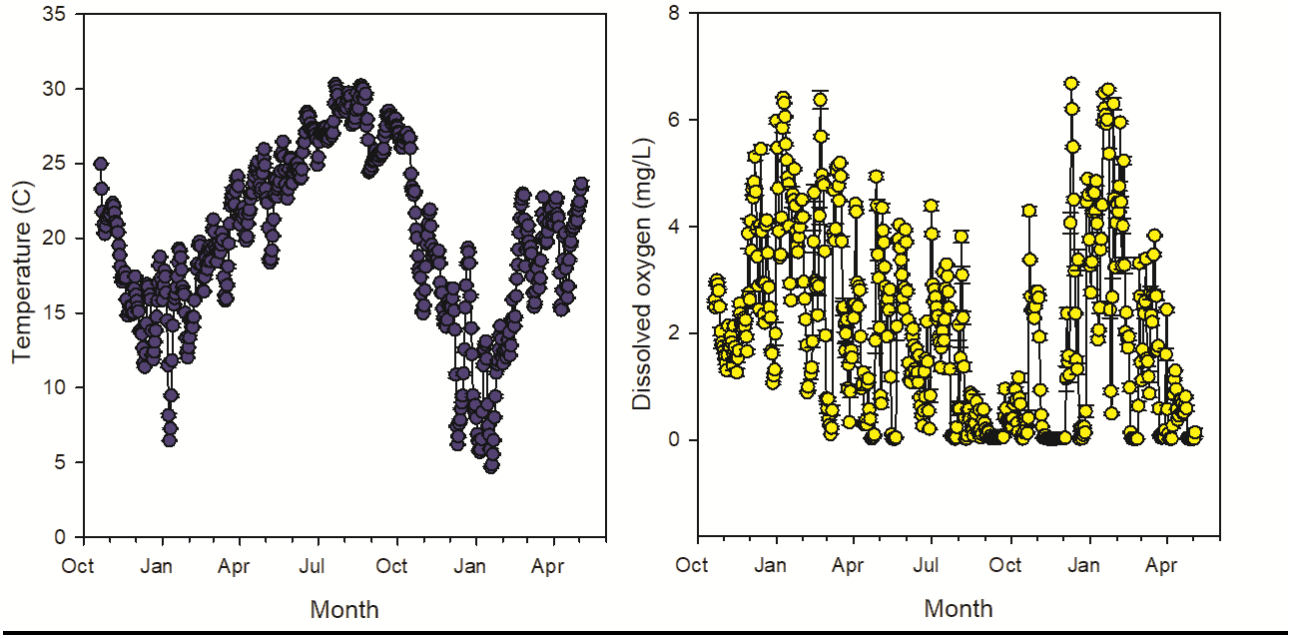

Figure 4. Daily mean temperature and oxygen concentration Grosse Tete (GT) Bayou from 2016 - 2017.

In GT Bayou, oxygen concentrations were low < 4 mg/L until December, after which there were greater fluctuations in DO with higher concentrations overall, likely associated with lower temperatures. Daily mean fluctuations in DO were high throughout the winter, spring and into the late summer. A period of continuous extreme low oxygen occurred from July –November 2017 becoming high and variable through the winter (**Figure 4**).

Water column nutrients

Three surface water samples were collected in June 2017 in the CT and GT for nitrate-nitrite-N, NO_3^--NO_2^--N), ammonium-N (NH_4^+) and soluble reactive phosphorus concentrations (SRP). Surface water nitrate concentration averaged 5 uM higher in GT than in CT ($p < 0.0001$), while both ammonium-N and SRP were significantly greater in CT than GT (**Figure 5**)

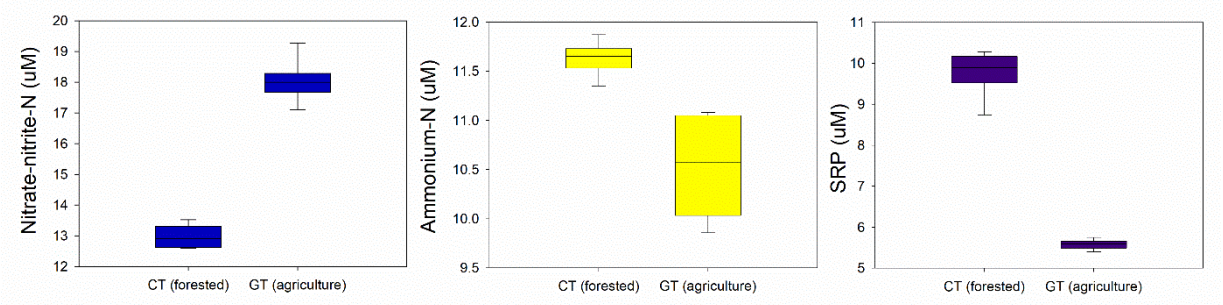

Figure 5. Surface water nutrient concentrations in the forested Choctaw Bayou (CT) and in the agricultural Grosse Tete (GT) Bayou.

Total organic carbon in surface water was highly variable in GT but was significantly greater in CT ($p = 0.0418$, **Figure 6**).

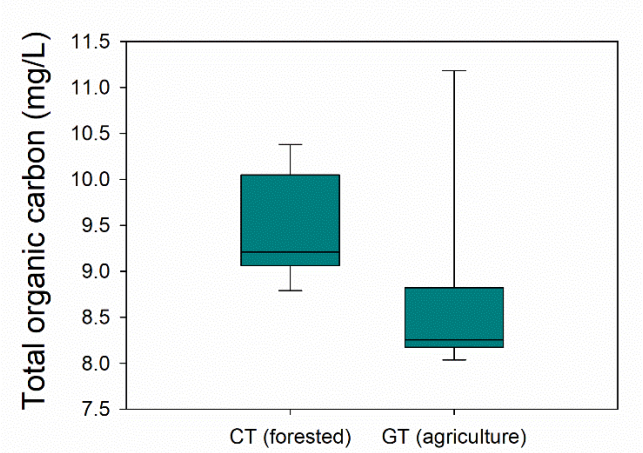

Figure 6. Total dissolved organic carbon in surface water of CT and GT in June 2017.

Oxygen consumption

Sediment and water (filtered and unfiltered) were oxygenated and then incubated in the lab at in-situ temperatures for measurement of oxygen consumption. All samples had initial DO concentrations around 10 mg/L, which declined linearly over time. In the sediment samples, DO tended to decline at a faster rate with oxygen concentrations generally reaching close to 0 mg/L by 1200 hrs after the start of the experiment (**Figures 7 and 8**). DO decline was slower in both filtered and unfiltered water. Filtering water had little effect on DO consumption rate, thus respiration may be occurring by smaller organisms. Most of the oxygen consumption occurred in the sediments (~50 mg/m^2/hr) from both bayous (**Figure 9**). There was no difference between bayous in the location and magnitude of oxygen consumption (**Figure 9**).

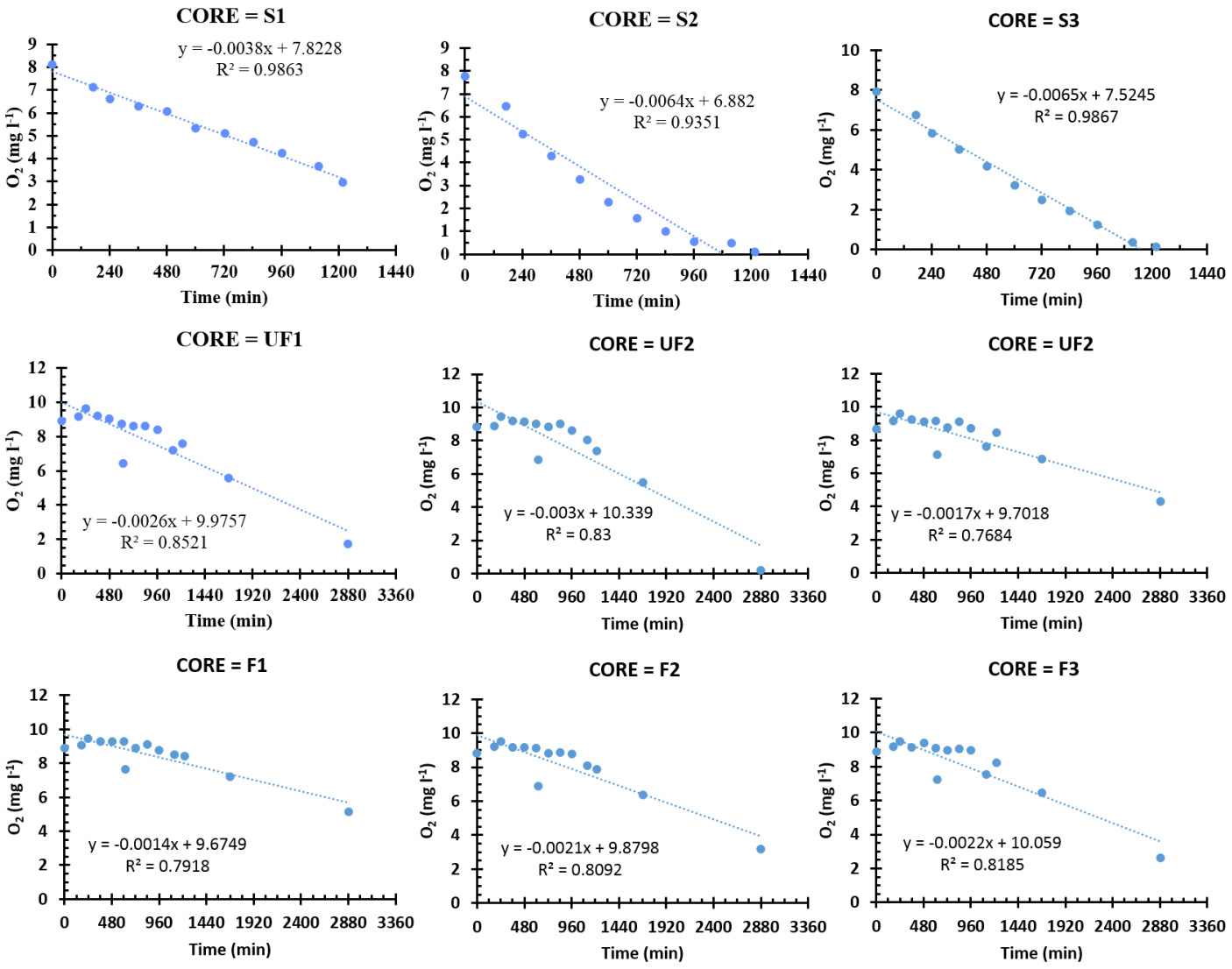

Figure 7. Time series oxygen concentrations in sediment, and unfiltered and filtered water from Choctaw Bayou.

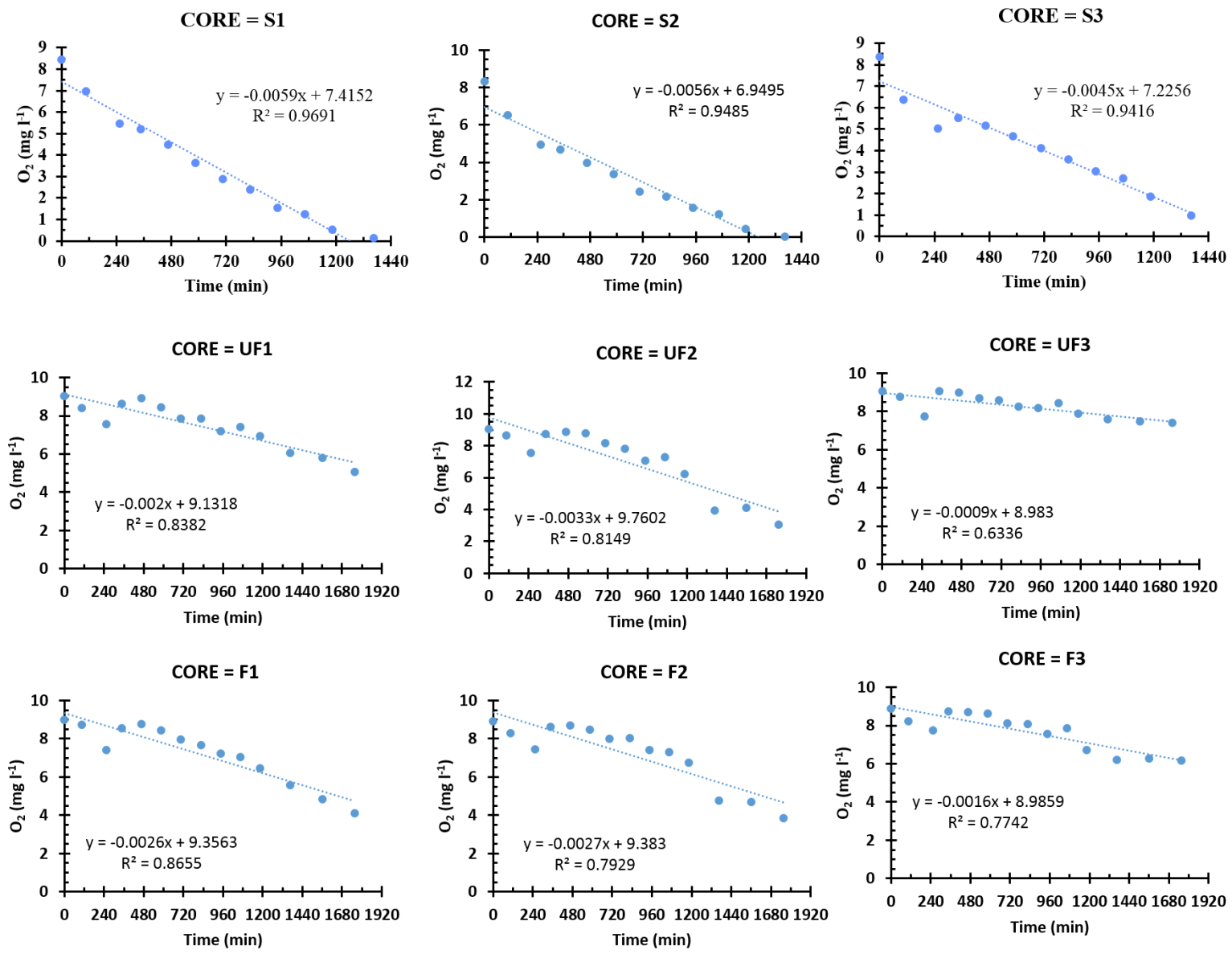

Figure 8. Time series oxygen concentrations in sediment, and unfiltered and filtered water from Gross Tete.

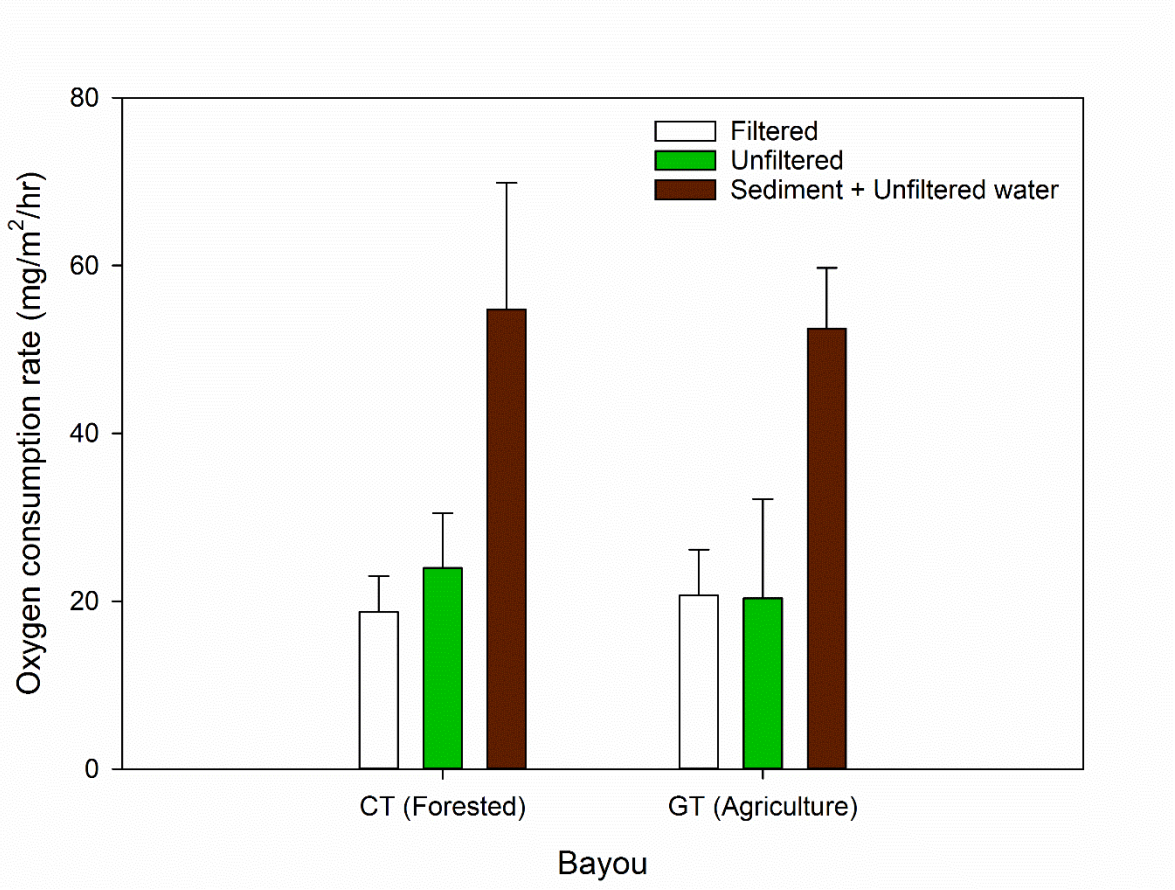

Figure 9. Average DO consumption rate across samples in two bayous surrounded by different land-use.

Summary and Significance

Five of the eight bayous had hypoxic conditions throughout the vertical depth profile. Three of the eight had DO concentrations between 2 and 6 mg/L within the top 1 m depth. Most of the DO consumption was occurring in the sediments not the water column. Diurnal and seasonal fluctuations in DO were apparent from continuous oxygen sensor data. Maximum DO concentrations were greater in the bayou surrounded by bottomland hardwood forest than the bayou surrounded by agriculture. Under controlled conditions, oxygen consumption rates were similar among the two bayous, and therefore, differences in other limiting factors or photosynthesis likely play a role in influencing differences in temporal DO dynamics. Small bayous provide important habitat for fish and other species and low oxygen conditions that can develop in the summer can limit aquatic organism distribution and survivorship.

References

Hladyz, S., S.C. Watkins, K.L. Whitworth, and D.S. Baldwin. 2011. Flows and hypoxic blackwater events in managed ephemeral river channels. Journal of Hydrology 401: 117-125.

Meyer, J.L., Perdue, E.M., Gjessing, E.T., 1990. Production and Utilisation of Dissolved Organic Carbon in Riverine Ecosystems. John Wiley and Sons Ltd, Chichester.

Sabater, S., J. Armengol, E. Comas, F. Sabater, I. Urrizalqui, and I. Urrutia. 2000. Algal biomass in a disturbed Atlantic river: water quality relationships and environmental implications. Science of the Total Environment 263: 185-195.

Sabo, M. J., C. F. Bryan, W. E. Kelso, and D. A. Rutherford. 1999. Hydrology and aquatic habitat characteristics of a riverine swamp: II. Hydrology and the occurrence of chronic hypoxia. Regulated Rivers: Research and Management 15: 525-542.

Tramer, E.J. 1977. Catastrophic mortality of stream fishes trapped in shrinking pools. American Midland Naturalist 97: 469–478.

Wagner, R.J., Boulger, R.W., Jr., Oblinger, C.J., and Smith, B.A., 2006, Guidelines and standard procedures for continuous water-quality monitors—Station operation, record computation, and data reporting: U.S. Geological Survey Techniques and Methods 1–D3,51p.+8attachments; accessed August 30, 2011, at *http://pubs.water.usgs.gov/tm1d3*

Whitworth, K.L., Baldwin, D.S., Kerr, J.L., 2012. Drought, floods and water quality: drivers of a severe hypoxic blackwater event in a major river system (the southern MurrayeDarling Basin, Australia). Journal of Hydrology 450-451: 190-198.

Economic Impacts of Groundwater Salinity in Louisiana Agriculture

Basic Information

Title:	Economic Impacts of Groundwater Salinity in Louisiana Agriculture
Project Number:	2016LA105B
Start Date:	3/1/2016
End Date:	2/28/2018
Funding Source:	104B
Congressional District:	LA-06
Research Category:	Water Quality
Focus Categories:	Agriculture, Economics, Irrigation
Descriptors:	None
Principal Investigators:	Krishna P. Paudel

Publications

1. Paudel, Krishna; Frank Tsai; Doleswar Bhandari; Matt Fannin, 2016, Assessing the economic impacts of salt water intrusion in an aquifer: a case of Mississippi River Valley Alluvial Aquifer, Louisiana, Challenges of Natural Resource Economics and Policy, 5th national forum on Socioeconomic Research in Coastal Systems March 20-22, New Orleans, LA.
2. Paudel, Krishna; Huizhen Niu; Dependra Bhatta; Frank Tsai, 2017, Using GIS to calculate crop area and water use in Louisiana 2004-2016, 2017 Southern Central Arc User Group and Louisiana Remote Sensing/GIS Conference, Baton Rouge, Louisiana, March 27-31.
3. Paudel, Krishna; Huizhen Niu; Dependra Bhatta; Frank Tsai, 2017, Evolution of irrigated crop areas and water use in Louisiana 2004 2016, 11th Annual Louisiana Groundwater, Surface Water, and Water Resources Symposium, Baton Rouge, Louisiana, April 11-12.
4. Karakullukcu; Ramazan, Dependra Bhatta; Frank Tsai; Krishna Paudel 2017 Construction of the Mississippi River Alluvial Aquifer, Northeast Louisiana, 11th Annual Louisiana Groundwater, Surface Water, and Water Resources Symposium, Baton Rouge, Louisiana April 11-12.
5. Biswo Poudel and Krishna P. Paudel. 2018. An Integrated Approach to Analyzing Risk in Bioeconomic Models. Forthcoming Natural Resource Modeling

Problem and Research Objectives

According to United States Department of Agriculture (USDA), roughly 56 million acres (7.6%) of all the U.S. cropland and pastureland were irrigated in 2012. The USDA survey-2010 has reported that of the total fresh groundwater withdrawals (76,000 Mgal/day), irrigation accounted for 65 percent of the total use. Nearly, all groundwater withdrawals (96 percent) were from freshwater.

Soybeans and feed grain production contributes significantly to Louisiana's economy. Most soybeans in Louisiana are produced in the Northeastern part of the state. Average soybean yield in 2014 was 57 bushels per acre and soybeans were produced in 1.39 million acres by 2509 producers in that year. The total economic contribution of soybean to the state is $1.2 billion. The region also produces significant amount of other grain crops such as corn, wheat and sorghum. The total value of these feed grain crops in the state are $396.4 million ($74.6 million for wheat, $37.9 million for sorghum, $298.1 million for corn).

Given that irrigation hedges the risk associated with an uncertain rainfall pattern, increasing numbers of farmers in the region are irrigating soybeans and other feed grains (except sorghum). In addition to hedge against the climate risk, farmers have been realizing significant increase in net revenue from irrigation even during normal years.

Many of top 10 soybean and feed grain producing parishes are located above the Mississippi River Valley Alluvial aquifer. Water in this aquifer has recently shown an increased salt concentration level. At the present Louisiana farmers can withdraw as much water as they need for irrigation. With the advent of polypipe, electric submersible pump, and laser leveling, the cost of irrigating crop fields has been substantially reduced. It is our observation that farmers are withdrawing as much water as needed to irrigate during the critical crop growth period of crops if they perceive that there is not enough rainfall since the last time they have irrigated the field.

Expansion of irrigated area and dependence on groundwater for irrigation in these crop growing areas have put enormous pressure on the Mississippi River Valley Alluvial Aquifer. In fact, farmers have been noticing higher concentration of salt in groundwater used for irrigation purpose. If continuous withdrawal of water is to be a norm, many fields are likely to have irrigation salinity problem that would result in build-up of salt in soil surface. Given groundwater is an open access resources, there is likely that social optimal may not be the private optimal withdraw. Further, without consideration of extractions by all users, there is likelihood that stock externality would persist. This means an individual farmer would withdraw more than necessary amount of groundwater.

This excessive withdrawal of water and resulting salinity problem may have far reaching adverse effects. Given agriculture is the mainstay of economy in the region, the region would suffer tremendous negative economic and social impacts. Benign impacts from soil salinity problem could be just changing the cropping system but at the extreme the whole region may be uncultivable in future. This would be clearly detrimental to the region and Louisiana Agriculture.

To overcome irrigation salinity, several measures can be taken. First, a comprehensive land water management plans should be developed. This means assessing all available water from groundwater and surface water in the region. Additionally, applying only the right amount of irrigation water that is sufficient for crops demand should be considered. Other land management practice that can help to reduce the adverse effects from soil salinity are using good soil management, avoiding deep tillage, and

adopting crop rotation measure. Similarly engineering measure such as subsurface tile drainage may help to capture water below the plant roots.

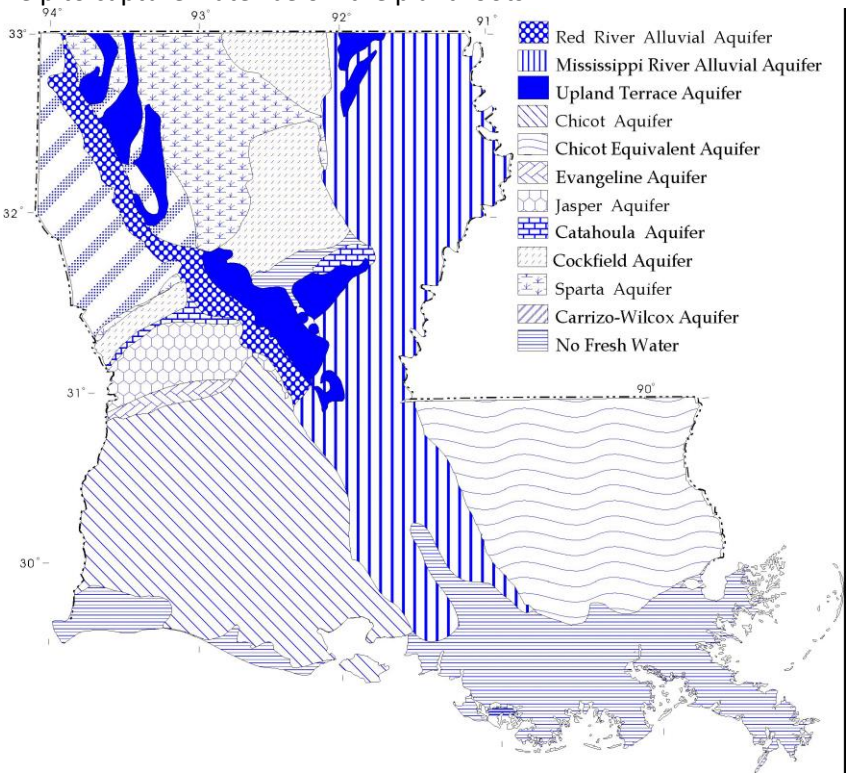

Figure 1. Louisiana aquifers – Mississippi River Alluvial Aquifer is the study region
(Figure source: USGS)

Objectives

1. Impact of salinity on crop production and overall economy of Louisiana
2. Assess the impact of sanity on groundwater extraction pattern

Methodology

1. Dynamic optimization model

Say a planner is solving an infinite horizon problem and has to decide the amount of harvest for each period. The parameters of the models are r (representing patience) and p (>0, net price per unit of harvest, considered to be fixed during the planning horizon). The primitive function of the model also includes $\lambda(s)$, a purely endogenous hazard (i.e., the probability of a catastrophe occurring when stock level is $s + \Delta s$, given that it has not occurred yet). The model is represented as:

$$\max_{\{h\}} \int_0^{\infty} e^{-rt} ph(t)dt$$

s.t.

$$\dot{s} = G\big(s(t)\big) - h(t),$$

$$s(0) = s_0;\ s(t) \geq 0, h(t) \geq 0 \ \forall \text{ t},$$

where $G(s(t)) = G_1(s(t))$ before the catastrophe, and $G(s(t)) = G_2(s(t))$ after the catastrophe. In this paper, catastrophe is defined as the one-time permanent shift in system dynamics, with the growth rate changing from $G_1$to G_2. In the paper by Polasky et al. (2011), $G_i(s)$ $= gs\left(1 - \frac{s}{K_i}\right), i = 1,2,$ (i.e., the source of the change in system dynamics is the change in carrying capacity).

In our example, fire destroys trees, and the lack of trees results in the likelihood of more erosion. Erosion in the forest affects the land area covered by the forest, which implies a reduction in K_i. This, in turn, results in a reduction in the maximum sustainable yield. There is only one catastrophe that can happen, post-catastrophe, there is no uncertainty in the model. The Hamilton-Jacobi- Bellman equation for the post-catastrophe value function V_2 is given by

$0 = max\{ph - rV_2(s) + V_2'(s)(G_2(s) - h)\}$.

Given the linearity of the control function, the solution to this equation is given by the following conditions:

(1) steady state s_2 satisfies $G_2'(s_2) = r$

(2) the value function and its derivative at s_2 are given by

$$V_2' = \begin{cases} \frac{pG_2(s_2)}{r} e^{-\int_s^{s_2} \frac{r}{G_2(\tau)} d\tau} & \text{for } s < s_2 \text{[1]} \\ \frac{pG_2(s_2)}{r} & \text{for } s = s_2 \\ e^{-rt_m(s)} \frac{pG_2(s_2)}{r} + \left(1 - e^{-rt_m(s)}\right) \frac{ph_m}{r} & \text{for } s > s_2, \end{cases}$$

where $t_m(s)$ is a solution of the function $t_m'(s) = \frac{1}{h_m - G_2(s)}$ and $V_2'(s_2) = p$.

(3) The optimal harvest rate is given by

$$h = \begin{cases} 0 & \text{for } s < s_2 \\ G_2(s_2) & \text{for } s = s_2, \\ h_m & \text{for } s > s_2 \end{cases}$$

where $h_m \to \infty$.[2]

The problem for the planner before the catastrophe is given by

$\max E\left\{\int_0^\tau e^{-rt} ph(t)dt + e^{-r\tau} V_2(s(\tau))\right\}$

s.t.

---

[1] Note that when $s < s_2$; $V_2'(s)G_2(s) - rV_2(s) = 0$, which is an ordinary differential equation for $V_2(s)$. Dividing both sides by $G_2(s)$ and multiplying by $e^{-\int_0^s \frac{r}{G_2(x)} dx}$, we get $e^{-\int_0^s \frac{r}{G_2(x)} dx} V_2'(s) - e^{-\int_0^s \frac{r}{G_2(x)} dx} \frac{r}{G_2(s)} V_2(s) = 0$. Since the left hand side is $\frac{d}{ds}\left[V_2(s)\, e^{-\int_0^s \frac{r}{G_2(x)} dx}\right]$, taking integration of both sides from 0 to s, and noting that $V_2 = 0$; and $V_2(s_2) = \frac{pG_2(s_2)}{r}$, which is the net present value of payoff pG_2S_2 for perpetuity, we get the solution.

[2] This is a standard result in the literature. One way to see this is as follows. Throughout this analysis, we assume the Benveniste-Scheinkman condition (Benveniste and Scheinkman, 1979) for the envelope theorem holds. Note that for $s < s_2$;$0 = -rV_2 + V_2'(s)G_2(s)$, and taking derivative with respect to s, we get, $V_2''(s) = (r - G_2'(s)) \frac{rV_2(s)}{(G_2(s))^2}$. The concavity of value function implies $r - G_2'(s) \leq 0$. Repeating same for s>s_2, we get $r - G_2'(s) \geq 0$, since $\frac{rV_2(s) - ph_m}{(G_2(s) - h_m)^2}$ is negative for $h_m \to \infty$. The continuity of $V_2''(s)$ then implies that $= G_2'(s_2)$.

$\dot{s} = G_1\big(s(t)\big) - h(t)$
$s(0) = s_0$
$s(t) \geq 0, h(t) \geq 0 \; \forall \, t$

Here τ is the time of arrival of catastrophe and is random by definition. As explained above, the catastrophe can be the result of either endogenous or exogenous risks or both. We first derive the expression for the hazard function using the arrival time of the catastrophe when the risk is purely endogenous, given that λ(s) is known.

Let $\Psi(t)$ define the probability that $\tau \leq$ t. Similarly, let F(s) and f(s) be the cumulative distribution and probability distribution corresponding to the hazard rate λ(s). It implies that 1-$\Psi(t) = prob(\tau \geq t | \tau > 0) = prob(s^* \geq s_t | s^* > s_0) = \frac{1-F(s_t)}{1-F(s_0)}$. This means the probability distribution function $\psi(t)$ is given by taking the derivative of the expression above: $\psi(t) = \frac{f(s_t)s}{1-F(s_0)} = \frac{f(s_t)}{1-F(s_0)}(G_1(s) - h)$. Hence the hazard rate associated with time is given by $\lambda_\tau(t) = \frac{\psi(t)}{1-\Psi(t)} = \frac{f(s_t)(G_1(s_t)-h)}{1-F(s_t)} = \lambda(s_t)(G_1(s_t) - h)$. We use this expression for the distribution of random variable τ to calculate the solution. Similarly, $\Psi(t) = \frac{F(s_t)-F(s_0)}{1-F(s_0)}$.[3] This expression allows us to write λ_τ using λ(s), which is assumed to be a primitive (given) function of the model.

In the first period, the planner solves the following problem:

$max E_\tau\left[\int_0^\tau e^{-rt} p h(t) dt + e^{-r\tau} V_2(s^c)\right]$

s.t.

$\dot{s} = G_1\big(s(t)\big) - h(t);$

$s(0) = s_0, s(t) \geq 0, h(t) \geq 0 \;\; \forall t$

Where s^c is the level of the state variable immediately after the catastrophe happens. Using Bellman's approach, we get the following expression for the value function

$w_1(s;t) = \max_h \left[\int_t^{t+\Delta t} e^{-rt} p h(x) dx + (1 - (\lambda_1 + \lambda_\tau)\Delta t) w_1(s + \Delta s, t + \Delta t) + (\lambda_1 + \lambda_\tau)\Delta t e^{-r(t+\Delta t)} V_2(s^c)\right]$

Using a standard dynamic theoretic approach, we now expand $w_1(s + \Delta s;\; t + \Delta t)$ around $(s;\; t)$; set λ_τ=λ (s)(G_1(s)-h); and use the expression that $\lim_{\Delta t \to 0} \frac{1}{\Delta t} \int_t^{t+\Delta t} e^{-rx} p h(x) dx = e^{-rt} p h(t)$. This gives

$0 = \max_h \{e^{-rt} p h(t) - (\lambda_1 + \lambda(G_1 - h)) w_1 + w_{1t} + [\lambda_1 + \lambda(G_1 - h)] e^{-rt} V_2 + W_{1s}(G_1 - h)\}$

Here, we have suppressed the arguments of w_1, λ, G_1, w_{1s}, w_{1t}.

Using a familiar method of transformation, we convert this into a time autonomous problem. Let $e^{rt} w_1(s; t) = V_1(s)$. Using this format, we replace w_1 (by $e^{-rt}V_1$); w_{1t} (by - re $^{-rt}V_1$), w_{1s} (by $e^{-rt}V_{1s}$) and we get

$0 = \max_h \{[p - V_1' + \lambda V_1 - \lambda V_2]h - \lambda_1 V_1 - \lambda G_1 V_1 - r V_1 + \lambda_1 V_2 + \lambda G_1 V_2 + V_1' G_1\}.$

We now make a convenient statement:

Lemma 1: *Suppose the following assumptions are made*:

[3] We haven't proven the fact that the state variable s_t would be monotonic over time. The proof is straightforward and relies on the arguments similar to those made in papers such as in Long (1978), Tsur and Zemel (1994), and Spraker and Biles (1996). Our calculation here follows a method similar to Tsur and Zemel (1994).

(a) Let Ω(s) = V_1(s)- V_2(s). Then $\Omega'(s) > 0, \lim_{s\to\infty} \Omega(s) \to 0. (b) \lim_{s\to\infty} V_1' > p\ (c) \lim_{s\to\infty} \lambda(s) \to 0. (d) \lim_{s\to\infty} V_1' = 0. Then\ there\ exists\ a\ unique\ root\ of\ f(s) = p - V_1' + \lambda V_1 + \lambda V_2.$

Proof: Note that $\lim_{s\to 0} f(s) > 0$. Since $\lim_{s\to\infty} \lambda(s) \to +\infty$, using (d), it is clear that $\lim_{s\to\infty} f(s) > 0$. Continuity of f(s) then guarantees a root. Furthermore, since $f'(s) = -V_1'' + \lambda'(s)(V_1 - V_2) + \lambda(s)[V_1'(s) - V_2'(s)] > 0$, this function cannot have more than one real root.

The linear nature of our problem implies that the optimal *h* will be given by

$$h = \begin{cases} 0 & if\ \ p - V_1' + \lambda V_1 - \lambda V_2 < 0 \\ h^m & if\ \ p - V_1' + \lambda V_1 - \lambda V_2 > 0 \\ h^s & if\ \ p - V_1' + \lambda V_1 - \lambda V_2 = 0\,. \end{cases}$$

Lemma 1 enables us to assume there exists a state s_1, such that when $s < s_1$ the policy is $h = 0$, and when $s > s_1, h = h^m$, where h^m indicates the maximum allowable harvest rate. This assumption implies that $p - V_1'(s) + \lambda(s)V_1(s) - \lambda(s)V_2(s^c) < (>)0$ when $s < (>)s_1$. The policy is a singular when $s = s_1$.

Hence the value function, V_1(s), is given by

$0 = \lambda_1(V_2 - V_1) + \lambda[G_1V_2 - G_1V_1] + V_1'G_1 - rV_1 \quad for\ s < s_1$ **(I)** and

$0 = [p - V_1' + \lambda V_1 - \lambda V_2]h^m + \lambda_1(V_2 - V_1) + \lambda(G_1V_2 - G_1V_1) + V_1'G_1 - rV_1 \quad for\ s > s_1$ **(II)**

Assuming that the value function is continuously differentiable, we can take **(I)** and **(II)** as two independent equations satisfying both **(I)** and **(II)** at $s = s_1$, and solve for $V_1(s_1)$ and $V_1'(s_1)$. The solutions are

$V_1(s_1) = \frac{\lambda_1 V_2 - \lambda G_1 V_2 + pG_1 - V_2 G_1}{r + \lambda_1}$ **(III),** and

$V_1'(s_1) = \frac{(r + \lambda_1 + \lambda G_1)V_1 - (\lambda_1 + \lambda G_1)V_2}{G_1}$ **(IV)**

If we were to know s_1, then **(III)** and **(IV)** would give an expression for the value function at $s = s_1$. Moreover, differentiating **(I)** and **(II)** with respect to s, we get,

When $s < s_1$,

$$G_1(s)V_1''(s) = rV_1'(s) - V_1'G_1' - \lambda[G_1V_2' + G_1'V_2 - G_1V_1' - G_1'V_1 - \lambda'[G_1V_2 - G_1V_1] - \lambda_1(V_2' - V_1') \quad \textbf{(V)}$$

When $s > s_1$,

$$[G_1(s) - h^m]V_1''(s) = -[\lambda'V_1 + \lambda V_1' - \lambda'V_2 - \lambda V_2']h^m + rV_1'(s) - V_1'G_1' - \lambda[G_1V_2' + G_1'V_2 - G_1V_1' - G_1'V_1] - \lambda'[G_1V_2 - G_1V_1] - \lambda_1[V_2' - V_1'] \quad (\boldsymbol{VI})$$

$Let\ \mathcal{L}_1(s) = (\lambda V_1' + \lambda' V_1 - \lambda V_2' - \lambda' V_2)$

$and\ \mathcal{L}_2(s) = rV_1'(s) - V_1'G_1' - \lambda[G_1V_2' + G_1'V_2 - G_1V_1' + G_1'V_1] - \lambda'[G_1V_2 - G_1V_1] - \lambda_1(V_2' - V_1')$.

Lemma 2: If $\lambda'(s) > 0,\ \mathcal{L}_1(s) > 0 \forall s, then\ the\ necessary\ condition\ for\ \mathcal{L}_1(s) \leq 0\ is\ \lambda'(s) < 0$.

Proof: It should be obvious, noting that

$\mathcal{L}_1(s) = \frac{d}{ds}\ [\lambda(V_1 - V_2)] = \frac{d}{ds}[\lambda\Omega] = \lambda\Omega' + \lambda'\Omega$. We know $\lambda, \Omega,$ and Ω' are strictly positive. Hence unless $\lambda' < 0, \mathcal{L}_1(s) > 0$. Note, however, that $\lambda' < 0$ is necessary but not sufficient condition for $\mathcal{L}_1(s) \leq 0$. By observing **(V)** and **(VI)**, it is clear that the concavity of V_1 would imply (i) The right hand side of **(V)** is

negative at $s \leq s_1$, and (ii) the right hand side of **(VI)** is positive at $s \geq s_1$.[4] Furthermore, notice that from Lemma 2,

$\mathcal{L}_1(s) > 0$; because $\lambda'(s) > 0$ [by assumption], which trivially implies that $\lambda'(s) > -\lambda \frac{V_1' - V_2'}{V_1 - V_2}$.

Taking the limit from the left, we get $\lim_{s \to s_1^-} V_1'' = \lim_{s \to s_1^-} \frac{\mathcal{L}_2(s)}{G_1(s)}$, and taking limit from the right, we get $\lim_{s \to s_1^+} V_1'' = \lim_{s \to s_1^+} \frac{\mathcal{L}_2(s) - \mathcal{L}_1(s) h^m}{G_1 h^m}$. Assuming that the limit exists at $s = s_1$, and allowing for $h^m \to \infty$, we get

$G_1(s_1) = \frac{\mathcal{L}_2(s_1)}{\mathcal{L}_1(s_1)}$ **(VII)**

This expression is valid, since by assumption $\mathcal{L}_1(s_1) > 0$. Now replacing $\mathcal{L}_2$ and $\mathcal{L}_1$, by their definition, we get

$G_1 = \frac{rV_1'(s) - V_1'G_1' - \lambda[G_1V_2' + G_1'V_2 - G_1V_1' + G_1'V_1] - \lambda'[G_1V_2 - G_1V_1] - \lambda_1(V_2' - V_1')}{\lambda V_1' + \lambda' V_1 - \lambda V_2' - \lambda' V_2}$ **(VIII)**

Upon further simplification, we get

$[G_1' - r - \lambda_1]V_1' = \lambda G_1' V_1 - \lambda G_1' V_2 - \lambda_1 V_2'$ **(IX)**

From (**VIII**), we know that in the limiting case when $\lambda(s)$ and λ_1 are identically zero, $G_1'(s_1) = r$, which is the standard solution in the absence of risk.

We also note that all functions in (**IX**) are known as the values of V_1, V_2, V_1', and V_2' have all been calculated previously.

Equation (**IX**) provides a framework to compare the steady state solutions under endogenous risk. First, notice that (**IX**) can be written as

$G_1' = \frac{rV_1' + \lambda_1(V_1' - V_2')}{V_1' - \lambda(V_1 - V_2)}$ **(X)**

Our discussion of the precautionary principle for endogenous risk rests crucially on (**X**).

(i) First, it is clear that in the absence of exogenous risk, the impact of endogenous risk is to increase the value of G_1', and hence decrease the level of steady state that the planner would be in if there were no such risk. Since

$V_1 - V_2 > 0$, (since the dynamics is assumed to be changing for worse, by definition V_2 should be less than V_1), it is clear that the impact of endogenous risk (or its increase) is unambiguously in favor of precaution. (To avoid the negative value of the steady state, we assume the denominator is not negative). In the forest management problem, it is implied that the risk of catastrophic wildfire causes decision makers to maintain a less steady state stock of forest, if they believe more trees will increase the hazard of wildfire. Precaution (or the propensity to stay farther away from the unknown threshold point triggering catastrophe) is an unambiguous result.

(ii) When the system faces the risk of extinction, i.e., $V_2 = V_2' = 0$, a situation much studied in the literature, mainly under the topic of irreversible catastrophe and also called *stock effect*, (**X**) becomes $G_1' = \frac{rV_1' + \lambda_1 V_1'}{V_1' - \lambda V_1}$. By dividing the numerator and denominator of the right hand side by V_1', this can also be written as

$G_1' = \frac{r + \lambda_1}{1 - \lambda\left(\frac{V_1}{V_1'}\right)}$ **(XI)**

[4] We assume V_1 is concave here.

Since this is the condition that needs to be satisfied in the steady state, intuitively, it is easy to see that the role of exogenous risk, *in the presence of endogenous risk*, when there is stock effect, is to increase precaution, as it increases the numerator. To see this, we note that the relationship between $V_1$and V_1' at $s = s_1$, when $V_2 = 0$ is given by $\frac{V_1}{V_1'} = \frac{1}{\lambda}\left(1 + \frac{p}{V_1'}\right)$, since at singular solution $p - V_1' + \lambda V_1 = 0$ when $V_2 = 0, V_1' > p > 0$. Hence $\frac{V_1}{V_1'} > 0$. In that case, (**XI**) can be rewritten as $G_1' = \frac{r+\lambda_1}{(p/m_1(s_1))}$, where $m_1(s_1)$ is the shadow price evaluated at steady state. If the market price reflects the shadow price, i.e., in case of no market failure, we get $G_1' = r + \lambda_1$, the result often found in the literature. This is an unambiguous result.

This is an important distinction from (i), and from previous studies in the literature in general. This implies that when there are both endogenous and exogenous risks, the risk of catastrophe won't lead people to act recklessly, and people actually react by increasing their precaution, especially if the market is pricing the resources precisely. Ambiguity is possible if resources are not priced accurately. The result in (i) was unconditional, the result here is not.

(iii) When there is no stock effect, the impact of exogenous risk, *in the presence of endogenous risk*, is ambiguous if the sign of $V_1' - V_2'$ is not constant. It crucially depends on which state the system will be in after the change in
the dynamic system. Suppose that post-catastrophe, the system moves to the state $s < s_2$. If after the catastrophe, the value function is believed to grow fast, whereas at the current state, the growth is comparatively stagnant, a not implausible scenario, the planner may not exercise precaution, especially since (a) she believes that the risk is exogenous and (b) though the transition is to a less desirable state, the growth rate in the less desirable state is higher than the growth rate she is in. If the planner believes that the risk is purely exogenous and that she could possibly do nothing to mitigate it, she is likely to be unworried, but if she knows further that the catastrophe will lead to a growth friendly state, she will be more upbeat and throw the caution away. However, for that to happen, the post-transformation marginal value function must be higher than pre catastrophe marginal value function.

(iv) The impact of exogenous risk *in the absence of endogenous risk* can't be analyzed by using **(X)**, since derivation of **(X)** relies on **(VII)**. In the absence of endogenous risk, $\mathcal{L}_1(s) = \lambda V_1' + \lambda' V_1 - \lambda V_2' + \lambda' V_2 = 0$, and this implies that **(VII)** is not a valid expression. However, the concavity of value function implies that the right hand side of equation **(V)**, namely $\mathcal{L}_2(s)$, must be negative when $s < s_1$, and positive when $s > s_1$. Therefore at the steady state, $s = s_1, \mathcal{L}_1(s) = 0$, which, using $\lambda = \lambda' = 0$, implies that, at $G_1' = \frac{rV_1'(s) + \lambda_1(V_1' - V_2')}{V_1} = r + \lambda_1\left(1 - \frac{V_2'}{V_1'}\right)$.

This gives the *increase in exogenous risk implies an increase in discount rate* type result, found in Yaari (1965), Reed (1984) and many other papers in the literature. However, the expression above implies that the results of Yaari (1965) are special case of our model, and is valid when $V_2' = 0$ (i.e., when the catastrophe implies $V_2 = 0$ in all states). This is the opposite of the precautionary principle, but is often justified by claiming that people respond to exogenous risk by overexploiting resources since there is nothing they can do to prevent the catastrophe. It is also clear that in general, the value inside the parenthesis depends on the specification of both V_1 and V_2.

2. *Input-output analysis*

We assume 5% loss in crop yield due to water salinity. It is possible to have more than 5% yield loss. Economic impact has linear effects. We calculated economic impact is using IMPLAN software.

Principal Findings and Significance

- Two kinds of risk are prevalent. Endogenous risk is created by human action. Exogenous risk is created by nature.
- Endogenous risk can be minimized by taking several actions. If there is only endogenous risk, resource managers should take precaution in extracting the resources.
- Managers should take precaution in extracting resources if there are both endogenous and exogenous risk and if there is stock effect. Without stock effect, results are ambiguous.
- If there is only exogenous risk, managers can do nothing. Therefore, managers should allow for the depletion of resources.
- Effects of salinity on economy can be serious if yield decline due to salinity is high or if farmers cannot substitute alternative crops for existing cropping pattern.
- If there is 5% reduction in crop yield, the impact on employment, labor income, and output be reduction of 675 jobs, $18.8 million, and $100 million reduction in output. The multiplier of unit reduction in total output. If this yield loss is higher than 5%, the impact would mulitiply accordingly. It can be very detrimental to Louisiana.

Grand total impact

5%	Employment	Labor Income	Output
Direct	-368	-$7,919,361	-$62,787,044
Indirect	-230	-$8,202,018	-$28,000,677
Induced	-77	-$2,693,300	-$9,308,013
Total	-675	-$18,814,679	-$100,095,734

Multiplier	1.83	2.38	1.59

Determination of chloride, nitrate and other ion concentrations in Mississippi Alluvial Aquifer in Northeast Louisiana

Basic Information

Title:	Determination of chloride, nitrate and other ion concentrations in Mississippi Alluvial Aquifer in Northeast Louisiana
Project Number:	2017LA112B
Start Date:	3/1/2017
End Date:	2/28/2018
Funding Source:	104B
Congressional District:	LA-06
Research Category:	Climate and Hydrologic Processes
Focus Categories:	Water Quality, Groundwater, Nutrients
Descriptors:	None
Principal Investigators:	Douglas alan Carlson

Publication

1. Douglas Carlson, 2017, Progress Report on Determination of Chloride, Nitrate and Other Ion Concentrations in Mississippi Alluvial Aquifer in Northeast Louisiana: NewsInsights, v. 27, p. 13-19.

Problem and Research Objectives

Problem

For most of northeastern Louisiana (Figure 1), the Mississippi River Alluvial Aquifer can account for over 90% of the groundwater supplied, the exception is Morehouse Parish. The Mississippi River Alluvial Aquifer in 2000, 2005 and 2010 accounts for 94% of all groundwater used in the nine parish study area (Sargent, 2002, 2007 and 2012) and 100% of groundwater used in three parishes: Franklin, Madison and Tensas and 2000 and 2005 (Sargent, 2002 and 2007). In the past fifty years groundwater use has increased in terms of the number of gallons (Figure 2) and increasing percentage of all water used in the nine parish study area from 50% in 1960 (Snider and Forbes, 1961) to 80% in 2010 (Sargent, 2012). This has been mainly being drive by a large increase in the number of acres of cropland irrigated within the study area from approximately 10,000 acres in 1959 to approximately 650,000 acres in 2012 (U.S. Department of Agriculture, 2016). There has even been slight increase in the share of groundwater used that is drawn from the Mississippi River Alluvial Aquifer from 89% in 1990 (Lovelace, 1991) to 93% in 2010 (Sargent, 2012)

Two reports have noted pockets of saltwater, as indicated by high chloride concentrations that lie in an axis from eastern Morehouse Parish to central Franklin Parish to central Concordia Parish (Whitfield, 1975; and Louisiana Department of Environmental Quality, 2003). The Louisiana Department of Environmental Quality (2003) study displays larger areas of higher chloride concentrations than Whitfield's (1975) study. However, this is could be a result of a smaller data set of only 25 wells rather than Whitfield's (1975) study, which includes samples from approximately 125 wells. The larger data set from the proposed study, when analyzed and mapped, should reveal the high chloride regions have expanded or not.

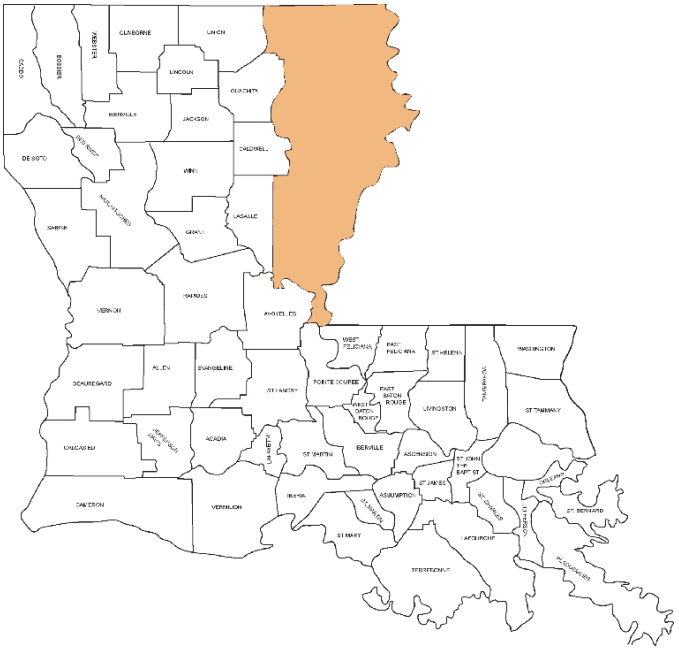

Figure 1. Location of study area.

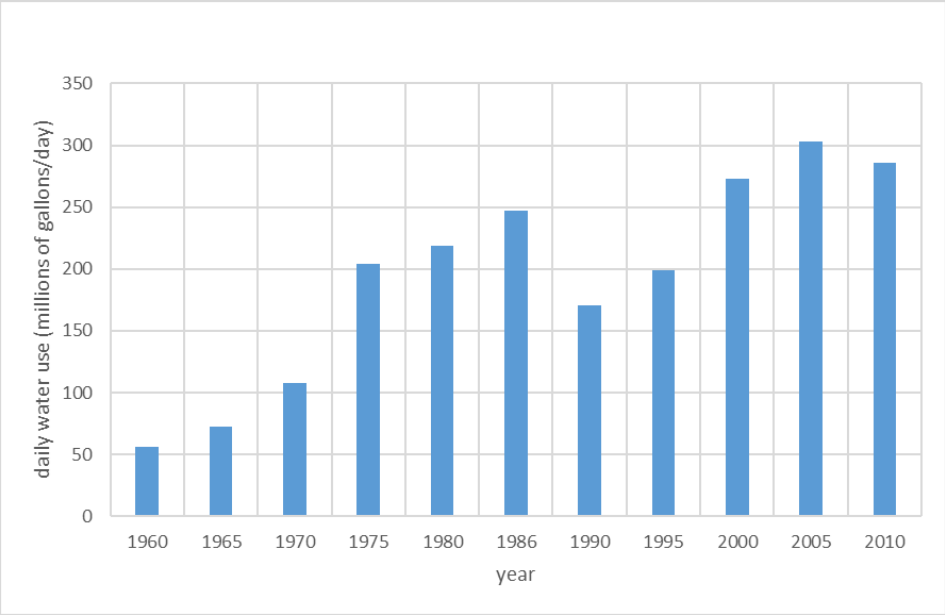

Figure 2. Daily groundwater use in study area between 1960 and 2010 (Snider, and Forbes, 1961; Bieber and Forbes,1966; Dial, 1970; Cardwell and Walter, 1979; Walter, 1982; Lurry, 1987, Lovelace, 1991; Lovelace and Johnson, 1996; and Sargent, 2002, 2007 and 2012).

Research Objectives

The proposed study will determine the distribution of chloride, nitrate and TDS concentration throughout a large portion of the Mississippi River Alluvial Aquifer that is most vulnerable to salinization and usually is under the greatest stress from pumpage. The last extensive study of water quality in Mississippi River Alluvial Aquifer was Whitfield's (1975). A small (only 25 wells) probably a quick study was completed by the Louisiana Department of Environmental Quality, 2003. However, the proposed study will be the first to consider the trend of chloride concentration in the Mississippi River Aquifer and mapping chloride and TDS concentrations with a density of observations similar to Whitfield's (1975). This study's results could be used to consider possible expansion/movement of the saltwater region over the past thirty-five years.

In terms of nitrate concentrations this is the first study since McGee's (1997) study of nitrate values in 1993 that included approximately 75 samples. The proposed study will have approximately twice as many samples and can be used to see if there is a general increase in nitrate concentrations between 1993 and 2009.

Methodology

Groundwater samples will be collected by the PIs after obtaining permission from the property owners. The water well will be purged as needed (approximately plumbing volume plus casing volume) prior to collection of the three samples that will be collected. Two samples will be in 50 ml-bottles. One will be preserved with nitric acid while the other one is unpreserved. The third sample will be in a 500-ml bottle and it will be unpreserved. All three

will be placed in a cooler with ice and keep at a temperature of approximately 4 ^{o}C in the field. Then the chilled samples will be stored in a refrigerator until analytical analysis.

Unpreserved 50 ml samples will be analyzed for anions and nutrients in the LGS laboratory. This analysis will be completed for the following: bromide, chloride, fluoride, nitrate, nitrite, phosphate, sulfate This analysis will be completed using LGS's Dionex ICS-1000 Ion Chromatography System as described in SM 9056A for determination of anions by ion chromatography (epa.gov, 2007). This technique is noted to have detections limit for these seven ions of 0.1 mg/L (NEMI, no date a) which is conservative as observed by the P.I. of this project. Peaks are clear often to concentration as low as approximately 0.05 mg/L.

In addition, the unpreserved 500 ml samples will be analyzed for TDS by gravimetric analysis, which involves using SM 160.1 gravimetric determination of TDS (caslab.com, 1971) in the LGS laboratory. Field measurements of specific conductance using LGS's Sper Scientific 850038 conductivity, TDS, salinity meter. Measurement of pH will involve using LGS's EcoSense pH100A meter.

Louisiana State University Wetland Biochemistry Service Laboratory will complete analysis for the metals and other cations. Metal/cation analysis will be completed using the lab's Varian (ICP-OES model MPX) Inductively Coupled Plasma-Optical Emission Spectrometer. This involves the use of the EPA 200.7-SW 846 6010B method which involves inductively coupled plasma-atomic emission spectrometry (caslab.com, 1996; and nelac-institute.org, 2008). Metals that are included in the analysis are aluminum, arsenic, barium, boron, cadmium, calcium, chromium, cobalt, copper, iron, lead, magnesium, manganese, nickel, phosphorous, potassium, selenium, silicon, silver, sodium, strontium, vanadium, and zinc. This analysis has detection limit of approximately 1 to 10 part per billion (ppb) depending on ion considered (caslab.com, 1996).

Principal Findings and Significance

Preliminary Results of this Study

At the time of this report samples have been collected and analyzed for wells in seven of the nine parishes within the study area: East Carroll, Franklin, Madison, Morehouse, Richland, Tensas, and West Carroll Parishes. Results for this study include analytical analysis in the laboratory for the concentrations of: aluminum, barium, boron, bromide, calcium, chloride, chromium, cobalt, copper, fluoride, iron, magnesium, manganese, nickel, nitrate, nitrite, phosphate, phosphorous, potassium, silicon, sodium, strontium, sulfate, vanadium, and zinc. In addition, field measurement were made for iron, nitrate, pH, phosphate, and specific conductivity, The first phase of this study has been largely completed with collection and analysis of domestic, irrigation, and stock wells, private systems. After the first phase is completed their be collection of a smaller number samples from public supply wells which tend to be the focus of previous studies such as: Whitefield, 1975, Seanor and Smoot, 1995; and Louisiana Department of Environmental Quality, 2003).

It is apparent even from this initial sample collection that Franklin and West Carroll Parish samples have far higher concentrations of chloride and Specific Conductivity than samples from elsewhere (Figure 3 and 4). Whitefield (1975) and Huff (1994) also noted this pattern earlier. The median concentration of chloride, 113 mg/L, is significantly higher than median observed for the LA DEQ studies (1999, 2003, 2006, 2009, and 2012), less than 40 mg/L. This could be a result of this studies greater share of samples in Franklin and West Carroll Parishes. However, it appears that this study's set of Franklin and West Carroll Parishes has larger chloride concentrations than Whitefield's (1975) for their select samples collected in just Franklin and West Carroll Parishes (Table 1). This study's results are similar to Whitfield's (1975) in Richland Parish This indicates that chloride concentrations are rising in Franklin and West Carroll Parishes which even the 1970s were already had greater concentrations than elsewhere within the Mississippi River Alluvial Aquifer (Whitefield, 1975).

The specific conductance results for this study are similar to past studies of Whitfield (1975) and McGee (1997) in Richland Parish (Table 2). For West Carroll Parish the specific conductance values have increased between Whitfield (1975) and McGee studies. Likewise, there has been a continuing increase in specific conductance between McGee (1997) and this study over the past twenty years. By contrast in Franklin Parish specific conductance has decreased between Whitfield (1975) and McGee (1997). Then trend between McGee (1997) and this study is not clear with mean continuing decrease, but median has increased.

Table 1
Chloride concentration for samples collected from wells in Richland and West Carroll Parishes for this study and Whitfield's (1975) study.

Study	No. of obs.	Mean	Median	Range
Franklin Parish				
Whitefield (1975)	33	88 mg/L	67 mg/L	17 to 270 mg/L
This study	35	163mg/L	132 mg/L	13.8 to 651 mg/L
Richland Parish				
Whitfield (1975)	15	92.2 mg/L	24.0 mg/L	1.0 to 960 mg/L*
This study	9	54.0 mg/L	26.3 mg/L	1.84 to 160 mg/L
West Carroll Parish				
Whitfield (1975)	18	46.2 mg/L	26.5 mg/L	2.3 to 123 mg/L
This study	15	143 mg/L	173mg/L	9.43 to 228 mg/L

The * notes the second highest concentration is only 150 mg/L.

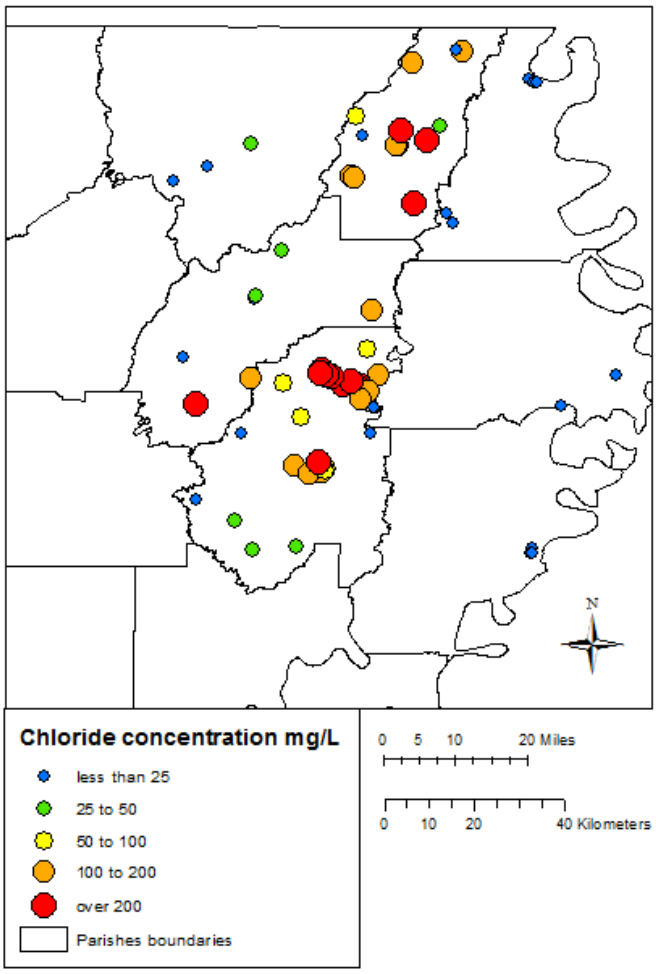

Figure 3. Initial observed values of chloride concentration within Mississippi River Alluvial Aquifer groundwater.

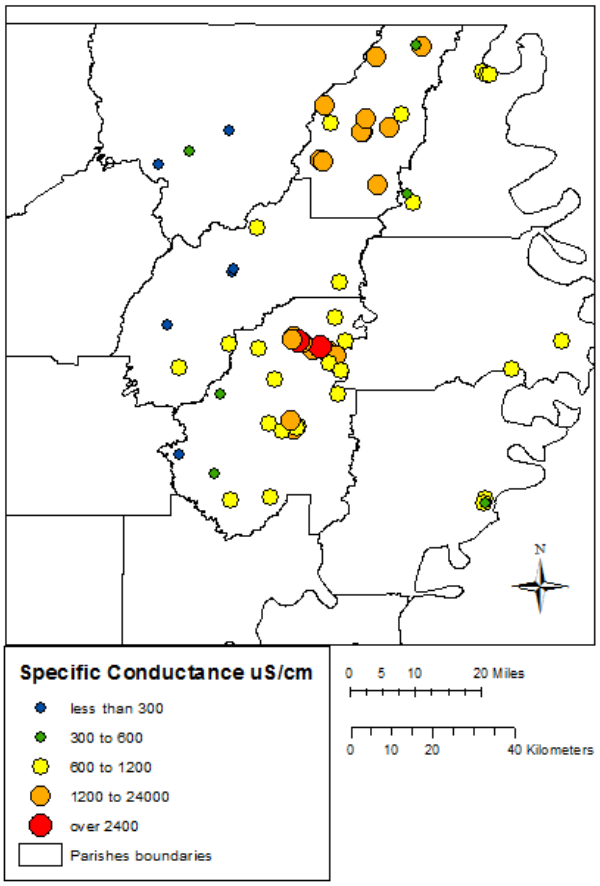

Figure 4. Initial observed values of Specific Conductance within Mississippi River Alluvial Aquifer groundwater.

Table 2
Specific conductance values for samples collected from wells in Richland and West Carroll Parishes for this study and two other large studies.

Study	No. of obs.	Mean	Median	Range
Franklin Parish				
Whitfield (1975)	33	1550 µS/cm	938 µS/cm	323 to 5520 µS/cm
McGee (1997)	22	1320 µS/cm	715 µS/cm	235 to 9940µS/cm#
This study	35	1100 µS/cm	935 µS/cm	239 to 2958µS/cm
Richland Parish				
Whitfield (1975)	13	631 µS/cm	443 µS/cm	117 to 2630 µS/cm*
McGee (1997)	15	540 µS/cm	385 µS/cm	102 to 1130 µS/cm
This study	9	532 µS/cm	483 µS/cm	35 to 1340 µS/cm
West Carroll Parish				
Whitfield (1975)	17	740 µS/cm	678 µS/cm	123 to 1290 µS/cm
McGee (1997)	10	1170 µS/cm	1210 µS/cm	722 to 1700µS/cm
This study	15	1410 µS/cm	1375 µS/cm	598 to 2320 µS/cm

The * notes the second highest value is only 1130 µS/cm. The # notes the second highest value is only 3560 µS/cm

In terms of nitrate, this is the first study since McGee's (1997) study of nitrate values in 1993 that included 83 samples. For this study's initial 75 values, most of which are in Franklin, Richland and West Carroll Parishes the results are very similar to McGee's (1997), see Table 3. This study there are three water samples with nitrate concentrations over U.S EPA standard, which is similar to McGee's (1997) results which included 2 out of the 83 wells sampled having nitrate values over the U.S. EPA standard.

Table 3
Nitrate concentration for samples collected from wells in Richland and West Carroll Parishes for this study and McGee's (1997) study.

Study	No. of obs.	Mean	Median	Range
Franklin Parish				
McGee (1997)	22	28.1 mg/L	0.93 mg/L	<0.09 to 133 mg/L
This study	35	11.7 mg/L	2.04 mg/L	<0.02 to 54.9 mg/L
Richland Parish				
McGee (1997)	15	2.91 mg/L	1.20 mg/L	<0.02 to 14.0 mg/L
This study	9	2.37 mg/L	1.59 mg/L	<0.02 to 8.56 mg/L
West Carroll Parish				
McGee (1997)	10	0.50 mg/L	<0.02 mg/L	<0.02 to 5.00 mg/L
This study	10	0.58 mg/L	0.10 mg/L	<0.02 to 2.40 mg/L

References

Bieber, P.P., and M.J. Frobes, Jr., 1966, Pumpage of Water in Louisiana, 1965: Department of Conservation Louisiana Geological Survey and Louisiana Department of Public Works: Water Resources Pamphlet, no. 20, 8p.

Cardwell, G.T., and W.H. Walter, 1979, Pumpage of Water in Louisiana, 1975: Louisiana Department of Transportation and Development Office of Public Works, Water Resources Special Report, no. 2, 15p.

Caslab.com, 1996, Method 6010B Inductively Coupled Plasma-Atomic Emission Spectrometry: http://www.caslab.com/EPA-methods/PDF/EPA-Method-6010B.pdf accessed June 17, 2016.

Caslab.com, 1971, SM 160.1 Residue, Filterable (Gravimetric, Dried at 180°C): http://www.caslab.com/EPA-Methods/PDF/EPA-Method-160-1.pdf accessed June 17, 2016.

Dial, Don C., 1970 Pumpage of Water in Louisiana, 1970: Department of Conservation Louisiana Geological Survey and Louisiana Department of Public Works, Water Resources Pamphlet, no, 26, 10 pg.

Gonthier, Gerard J., 2003, Quality of ground water in Pleistocene and Holocene subunits of the Mississippi River valley alluvial aquifer, 1998: U.S. Geological Survey Water-Resources Investigations 03-4202, 80 pg.

Huff, G.F., 1994, Geologic controls on elevated salinity in the Mississippi River alluvial aquifer of eastern Morehouse Parish, Louisiana, and southern Chicot County, Arkansas: Gulf Coast Association of Geological Societies, Transactions., v. 44, pg. 285-292.

Huff, G.F., and J.P. Bonck, 1993, Saltwater in Shallow Aquifers in East-Central and Northeastern Louisiana and Southeastern Arkansas: U.S. Geological Survey Open-File Report 93-494, 54p.

Kingsbury, James A., Jeannie R.B. Barlow, Brian G. Katz, Heather L. Welch, Roland W. Tollett, and Lynne S. Fahlquist, 2014, Water Quality in the Mississippi Embayment-Texas Coastal Uplands Aquifer System and Mississippi River Valley Alluvial Aquifer, South-Central United States, 1994-2008: U.S. Geological Survey Circular 1356, 84p.

Louisiana Department of Environmental Quality, 2012, Mississippi Alluvial Aquifer Summary 2008 Aquifer Sampling and Assessment Program: Louisiana Department of Environmental Quality, 2003, 31p

Louisiana Department of Environmental Quality, 2009, Mississippi Alluvial Aquifer Summary 2008 Aquifer Sampling and Assessment Program: Louisiana Department of Environmental Quality, 2003, 31p

Louisiana Department of Environmental Quality, 2005, Mississippi Alluvial Aquifer Summary Baseline Monitoring Project, FY 2005: Louisiana Department of Environmental Quality, 2006, 23p.

Louisiana Department of Environmental Quality, 2003, Mississippi Alluvial Aquifer Summary Baseline Monitoring Project, FY 2002: Louisiana Department of Environmental Quality, 2003, 24p.

Louisiana Department of Environmental Quality, 1999, Mississippi Alluvial Aquifer Summary Baseline Monitoring Project, EPA FY 99: Louisiana Department of Environmental Quality, 1999, 21p.

Lovelace, J.K., and P.M. Johnson, 1996, Water Use in Louisiana, 1995: Louisiana Department of Transportation and Development, Water Resources Special Report, no. 11, 127p.

Lovelace John K., 1991, Water Use in Louisiana, 1990: Louisiana Department of Transportation and Development, Water Resources Special Report, no. 11, 127 pg.

Lurry, D.L., 1987, Pumpage of Water in Louisiana, 1985: Louisiana Department of Transportation and Development, Water Resources Special Report, no. 4, 14p.

McGee, B.D., 1997, Occurrence of nitrate in the Mississippi River Alluvial Aquifer in Louisiana, June through December 1993: Louisiana Department of Transportation and Development, Water Resources Technical Report, no. 61, 21p.

Nelac-institute.org/docs, 2008, Auditing ICP Methods EPA 200.7, Rev. 4.4 SW-846 6010B: Nelac-institute.org/docs/meeting/newport2008/Auditing-an-ICP-method.pdf accessed June 17, 2016

Pettijohn, Robert A., 1992, Properties and chemical constituents in ground water from the Mississippi River valley alluvial aquifer and permeable zone A (Holocene-upper Pleistocene deposits) south-central United States: Water Resources Investigation no 91-4149, 5 plates.

Sargent B. Pierre, 2012, Water Use in Louisiana, 2010: Louisiana Department of Transportation and Development, Water Resources Special Report, no 17, 135 pg.

Sargent, B.P., 2007, Water Use in Louisiana, 2005: Louisiana Department of Transportation and Development, Water Resources Special Report, no. 16, 133p.

Sargent B. Pierre, 2002, Water Use in Louisiana, 2000: Louisiana Department of Transportation and Development, Water Resources Special Report, no 15, 133 pg.

Seanor, R.C., and C.W. Smoot, 1995, Louisiana Ground-Water Map no. 6: Water-Level Changes, 1974-90, of the Mississippi River Alluvial Aquifer in Northeastern Louisiana: U.S. Geological Survey Water Resources Investigations Report 95-4146, 2 sheets.

Snider, J.L., and M.J. Forbes Jr., 1961, Pumpage of Water in Louisiana, 1960: Louisiana Department of Public Works and Department of Conservation Louisiana Geological Survey, 6 pg.

U.S. Department of Agriculture, 2016, Census of Agriculture: http://www.agcenesus.usda.gov/Publications/2007/ accessed October and November, 2016.

U.S. Environmental Protection Agency, 2017, National Primary Drinking Water Regulations: United States Environmental Protection Agency, https://www.epa.gov/ground-water-and-drinking-water/national-primary-drinking-water-regulations#Inorganic Accessed November 28, 2017.

U.S. Environmental Protection Agency, 2007, Method 9056A Determination of Inorganic Anions by Ion Chromatography: United States Environmental Protection Agency, https://www.epa.gov/sites/production/files/2015-12/documents/9056a.pdf Accessed November 25, 2016.

Walter, W.H, 1982, Pumpage of Water in Louisiana, 1980: Louisiana Department of Transportation and Development, Water Resources Special Report, no., 3, 15 pg.,

Welch, Heather L., James A. Kingsbury, Roland W. Tollett, and Ronald C. Seanor, 2009, Quality of shallow groundwater and drinking water in the Mississippi Embayment-Texas Coastal Uplands aquifer system and the Mississippi River valley alluvial aquifer, south-central United States, 1994-2004: U.S, Geological Survey Scientific Investigations Report 2009-5091, 51 pg.

Whitefield, M.S., Jr., 1975, Geohydrology and Water Quality of the Mississippi River Alluvial Aquifer, Northeastern Louisiana: Louisiana Department of Public Works: Water Resources Technical Report, no. 10, 29p.

Effects of climate change on nitrogen and sulfur deposition to Louisiana water bodies using climate downscaling meteorology and chemical transport model

Basic Information

Title:	Effects of climate change on nitrogen and sulfur deposition to Louisiana water bodies using climate downscaling meteorology and chemical transport model
Project Number:	2017LA113B
Start Date:	3/1/2017
End Date:	2/28/2018
Funding Source:	104B
Congressional District:	LA-06
Research Category:	Climate and Hydrologic Processes
Focus Categories:	Acid Deposition, Models, Climatological Processes
Descriptors:	None
Principal Investigators:	Hongliang Zhang

Publications

1. Guo Hao, Fenglin Han, and Hongliang Zhang#. 2018. Effects of climate change and emissions on air pollution and its deposition in Southeast US. In preparation.
2. Guo Hao, Hongliang Zhang. 2018. Effects of climate change and emission scenarios on nitrate and sulfur deposition to surface water in Louisiana. 12th Annual Louisiana Groundwater, Surface Water and Water Resources Symposium, Louisiana State University, Baton Rouge, LA

Problem and Research Objectives

Louisiana has abundant water resources, with approximately 11% of the total surface area is composed of water bodies. The state has more than 40,000 miles of rivers, streams and bayous, and 400 miles of coastline. Almost every aspect of economy in Louisiana can be tied to the development and utilization of water resources. However, Louisiana water bodies are eutrophic and excess nutrients are driving regional problems such as hypoxia. In 2012, only 26% of Louisiana segments supported fishing and only 68% support swimming (DEQ, 2012). Thus, it is important to protect water resources from being worsened. Primary reasons for the water impairment include oxygen depletion and the interrelated problem of excess nutrients such as nitrogen (N) and phosphorus (P). Sulfur (S) deposition causes other forms of impairment including acidification.

Currently, Louisiana is undergoing an unprecedented industrial expansion in the driven by increased availability and cost of natural gas and petroleum products. Increased emissions from these activities are expected in future decades, which could contribute significantly to additional aquatic impairment. In addition, the climate is changing. The expected effects in Louisiana include higher temperature leading to stronger photochemical processes that change the formation and removal rates of N and S containing species (Bradley et al., 2010; Tai et al., 2010). Thus, the deposition of N and S in future maybe significantly changed.

The understanding of increased emissions and deposition of N and S under future changing climate is of great interest to regulators, industry and the academic community. This project will develop tools to estimate the effects of climate change on spatial deposition of N and S to Louisiana water bodies using climate downscaling meteorology and chemical transport model, which have not applied previously to these aquatic systems.

Thus, **the objective of this project** is to identify the changes in total fluxes and contributions of different source sectors and regions to S and N deposition due to changing emissions and climate including the forms and quantities by wet and dry processes, spatial and temporal distribution, and local and long-range transport splits.

Methodology

The Weather Forecasting and Researching model (WRF) and EPA Community Multiscale Air Quality (CMAQ) modeling system combined with evaluation and analysis using various observations were used to achieve the objectives proposed. Figure 1 shows an over-view of the compartmentalized project plan. The research is divided into following major research tasks.

- **Task 1**: Building the platform with climate downscaling meteorology.
- **Task 2**: Generating future emissions inventories.
- **Task 3**: Obtaining effects of emission and climate change on total S and N deposition.

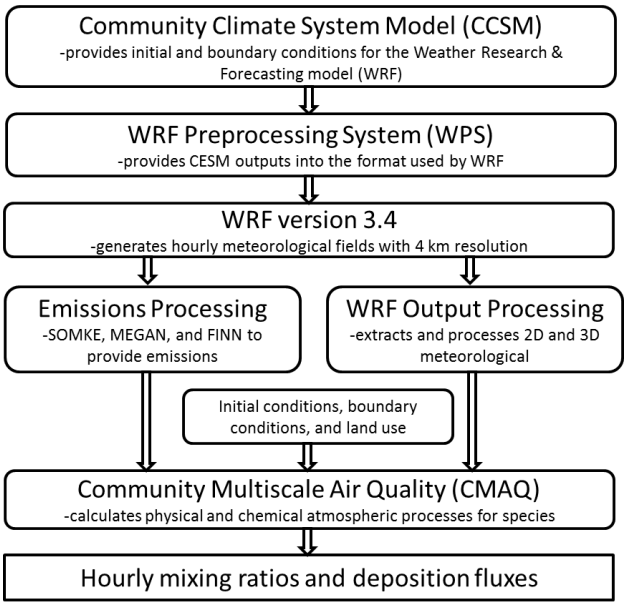

Figure 1. Flow chart of the climate downscaling and air quality modeling system.

Task 1: Building the platform with climate downscaling meteorology.

The EPA Community Multiscale Air Quality (CMAQ) modeling system is the tool in this study. It is a third generation air quality model that is designed for applications regulatory and policy analysis to understanding the complex interactions of atmospheric chemistry and physics (Byun and Schere, 2006). CMAQ is a community model with highly transparent code and modular configuration that facilitates the extensibility through community development by researchers worldwide. Nested domains are usually used for regional air pollution simulation. For this project, three nested domains shown in Figure 2 were used. The outer domain, 36km, covers the whole US, including the areas that may affect air pollution in Louisiana. 12km domain includes Southeast states, and 4km domain covers most part of Louisiana with the center on Baton Rouge and New Orleans. 36km domain uses typical boundary conditions and it provides boundary conditions for 12km domain while 12km domain provides boundary conditions for 4km domain.

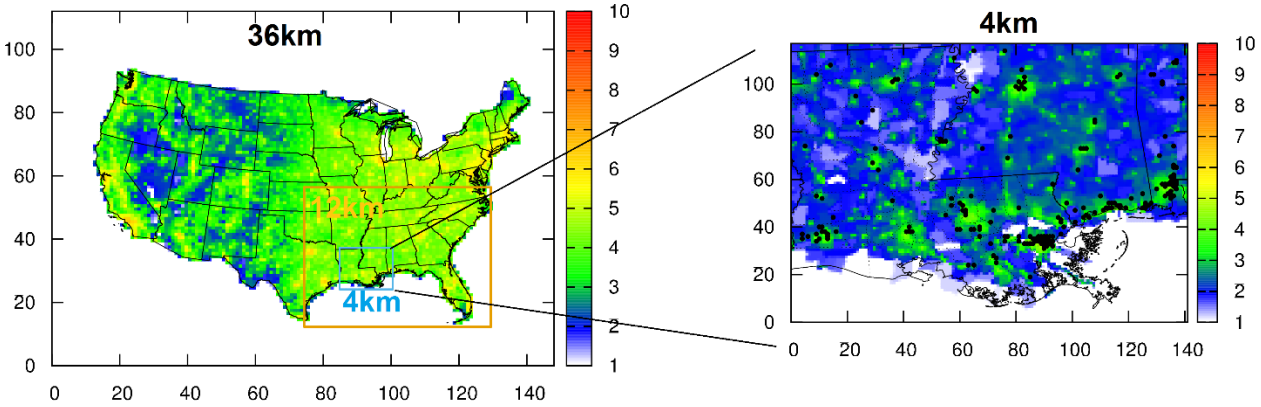

Figure 2. The designed nested domains for air quality simulation platform centered at Louisiana. Color shows the log of population in each grid. The black dots show the locations of observation sites.

Two types of inputs, meteorological information and emission rates from different sources, are needed for CMAQ simulation. The effects of climate act through the input of

meteorology. Meteorology plays significant role in fate of atmospheric pollutants since it not only affects their transport, diffusion, and deposition but also the chemical transformation by influencing the reaction processes. Results from one of global climate models (GCMs), Community Climate System Model (CCSM), were downscaled for future climate periods of 2050 based on three climate scenarios (RCP 4.5/6.0/8.5). Weather Research and Forecasting (WRF) model is a next-generation mesoscale numerical weather prediction system that is widely used nowadays for air quality models (Skamarock et al., 2008). The initial and boundary conditions for WRF simulations were prepared using WRF Preprocessing System (WPS) with GCM outputs instead of reanalysis to represent future climate. Meteorology-Chemistry Interface Processor (MCIP), which takes in meteorological outputs from WRF and prepares meteorological data needed for CMAQ, was used.

Task 2: Generating future emissions inventories.

Another input to CMAQ simulation is gridded emissions. National Emissions Inventory (NEI) from the Environmental Protection Agency (http://www.epa.gov/ttn/chief/eiinformation.html) was downloaded for use. The anthropogenic emissions for current years can be directly obtained and processed using Sparse Matrix Operator Kernel Emissions (SMOKE) Modeling System missions. For 2050 emissions, we conducted three set of simulations. No change case directly uses 2011 emissions to see the net effects of climate change, BAU case uses adjusted emissions in 2050 business as usual to get the effects of both emission/climate change, and controlled case uses Global Change Assessment Model (GCAM-USA) to get state-level prediction of future anthropogenic emissions based on potential emission control strategies by U.S.EPA. The method described in Woo et al. (2008) was adopted to adjust future emissions.

Biogenic emissions were generated using the Model for Emissions of Gases and Aerosols from Nature (MEGAN) v2.1. The leaf area index (LAI) were based on the 8-day Moderate Resolution Imaging Spectroradiometer (MODIS) LAI product (MOD15A2) and the plant function types (PFTs) were based on the PFT files used in the Global Community Land Model (CLM 3.0). For more details of the biogenic emission processing, the readers are referred to Qiao et al. (2015). Open biomass burning emissions were generated from the Fire INventory from NCAR (FINN), which is based on satellite observations (Wiedinmyer et al., 2011).

Task 3: Obtaining effects of emission and climate change on total S and N deposition.

First set of simulation conducted the present case for comparison with future cases. Then, the climate downscaling meteorology was used but the emissions were remained same as 2011. So the effects of climate change only were obtained. The third set of simulation used the future climate downscaling meteorology and the 2050 emissions inventory based on possible future economic boosting strategies in Louisiana. The fourth set of simulation used the future climate downscaling meteorology and the 2050 emissions inventory based on possible emission control strategies by U.S.EPA in Louisiana. According to this simulation, the effects of emission and climate change were obtained.

Principal Findings and Significance

Figure 3 shows the emission of $PM_{2.5}$, NOx, NH_3 and SO_2 under three emission scenarios in January 2050. Emissions in BAU case shows significant increase, while controlled case shows a decrease. The spatial distribution of $PM_{2.5}$ emission shows high emission at Mississippi and south Louisiana, while NOx emission distributes along the highways and seashore of southeast Louisiana as majority of NOx emission comes from vehicles emissions. NH_3 emissions have a

significant peak at central Louisiana near Baton Rouge. This area has ammonium plants in operation, so industry emissions should be the major sources. SO_2 emissions are higher along the bank of Mississippi River because high emission rates of SO_2 from power plants and chemical industry (Mudd, 2012).

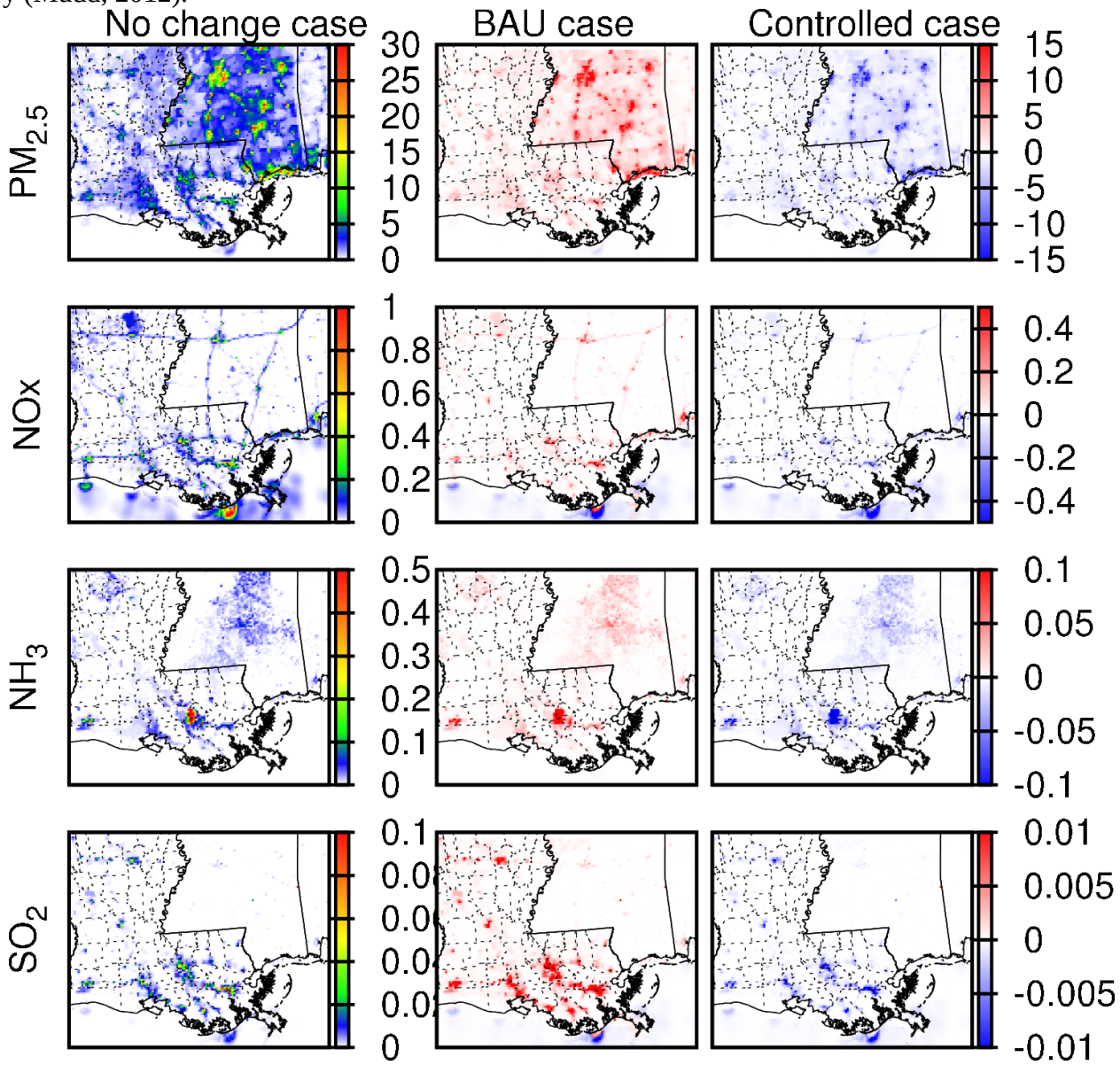

Figure 3. Monthly average emissions of no change case in January 2050 with the differences of BAU case and controlled case (Unit: mol/s except g/s for $PM_{2.5}$).

Figure 4 shows the emission of $PM_{2.5}$, NOx, NH_3 and SO_2 under three emission scenarios in August 2050. The emissions in August are very similar to January, but we can still identify some differences. The $PM_{2.5}$ emission is higher in August at northeast and southwest Louisiana while NH_3 emission is also higher in majority parts of Louisiana.

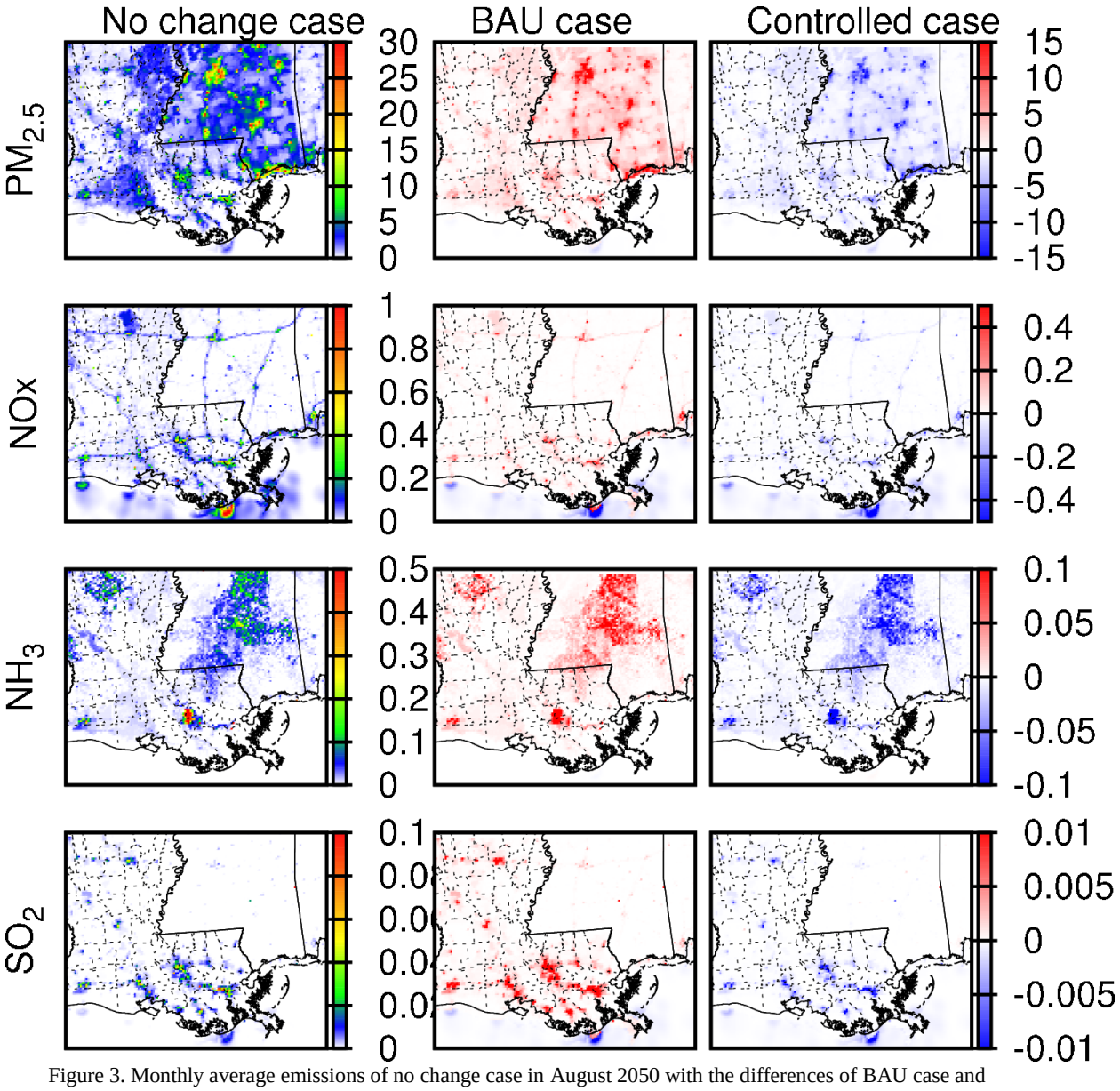

Figure 3. Monthly average emissions of no change case in August 2050 with the differences of BAU case and controlled case (Unit: mol/s except g/s for $PM_{2.5}$).

Figure 5 shows the future case in January and August 2050 with climate downscaling meteorology used and the emissions remained same as 2011. The no change case results shows an increase trend in August 2050 with total nitrogen and sulfur deposition in all three climate scenarios. The increase of relative humidity and temperature offers a suitable environment for sulfur and nitrogen species deposition to ground through both dry and wet depositions. Nitrogen depositions decrease in January 2050 under three climate scenarios. Nitrogen depositions peak with extremely high values up to 5 kg N/ha at central Louisiana near Baton Rouge. This area has ammonium plants in operation, so industry emissions should be the major sources. High sulfur deposition fluxes occurs at boundary of Louisiana in August 2050 at both three climate scenarios, which indicates a significant sulfur transported from adjunct states like Alabama, Mississippi and Texas.

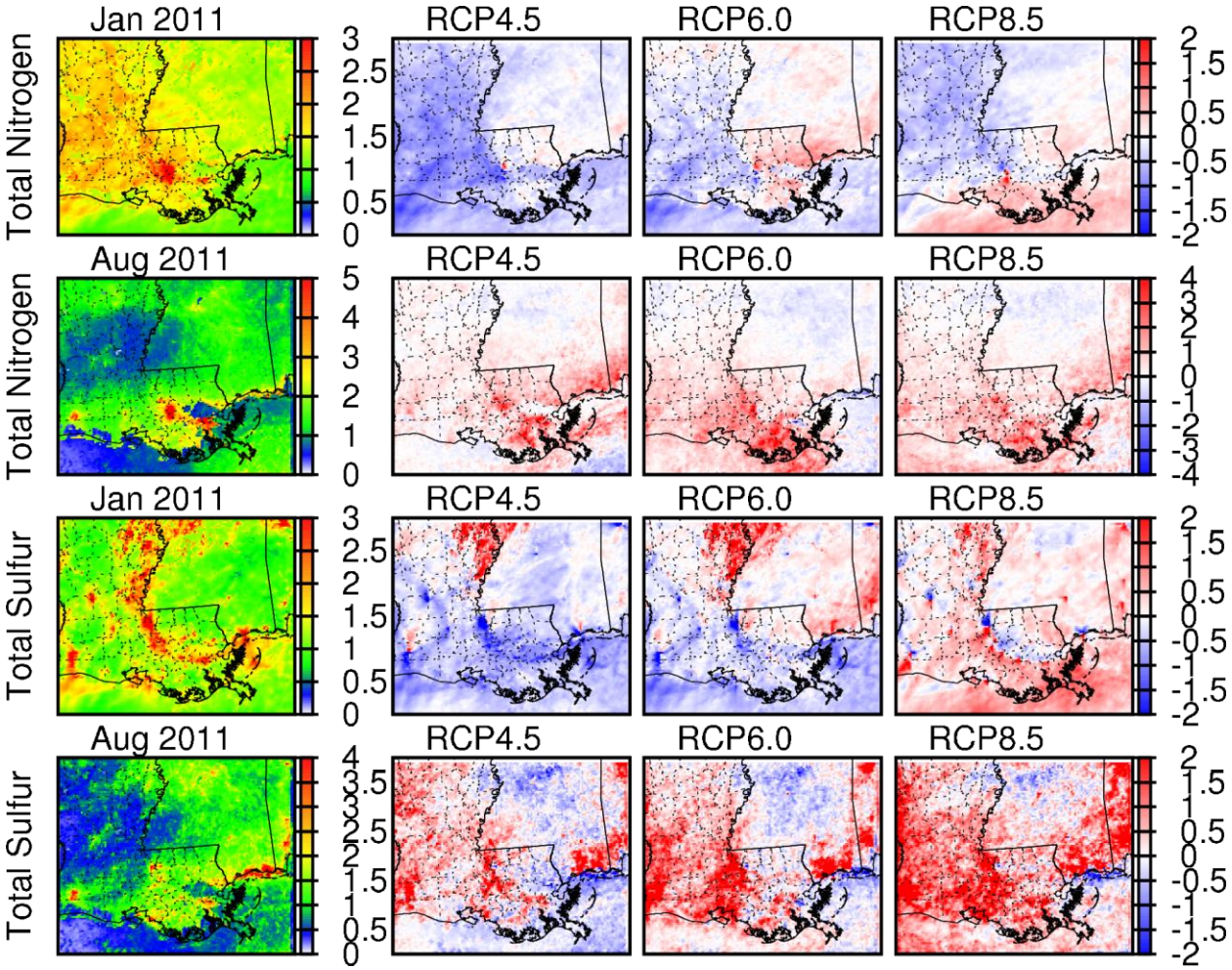

Figure 5. Total nitrogen and sulfur deposition fluxes in at Jan and Aug.2011 with the differences from 2050 to 2011 in RCP4.5/6.0/8.5 climate scenarios and no change case of emission scenario (Unit: kg S/ha).

Figure 6 shows the future case in January and August 2050 with climate downscaling meteorology used and adjusted emissions in 2050 based on a consistent increase assumption of business as usual. The BAU case shows an increase trend in most part of Louisiana in both nitrogen and sulfur depositions in January and August 2050 because the significant increase of emissions in BAU cases. In south Louisiana, nitrogen depositions decrease slightly in January 2050 in RCP4.5/6.0 climate scenarios. With long coastal line in south, the decrease probably relates to the land-sea breeze circulation occurring at winter seashore. Also, another slight decrease of nitrogen deposition occurs at north Louisiana under RCP8.5 climate scenario.

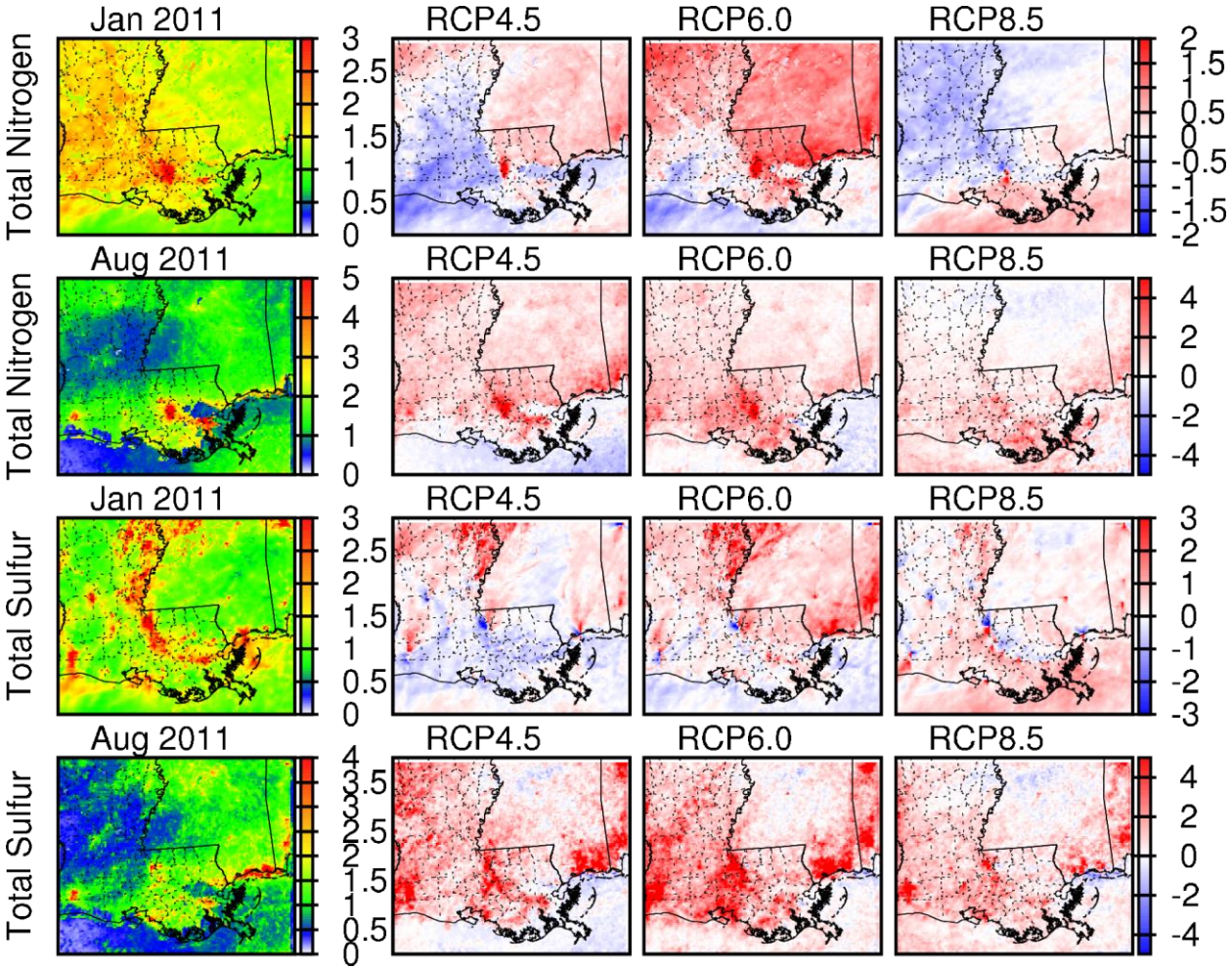

Figure 6. Total nitrogen and sulfur deposition fluxes in at Jan and Aug.2011 with the differences from 2050 to 2011 in RCP4.5/6.0/8.5 climate scenarios and BAU case of emission scenario (Unit: kg S/ha).

Figure 7 shows the future case in January and August 2050 with climate downscaling meteorology used and controlled emissions in 2050 based on prediction of Global Change Assessment Model (GCAM-USA). Due to controlling of anthropogenic emissions, nitrogen depositions show a decreasing trend in January and August 2050 of RCP 4.5/6.0/8.5 climate scenarios. Although the major parts of Louisiana shows a decreasing of sulfur deposition in January 2050, a significant increase occurs at northeast Louisiana. As the source apportionment results shows, the significant sulfur transport from north states of Louisiana could be the main reason. Also, the significant sulfur transport from Texas contributes to sulfur deposition in west Louisiana at August 2050.

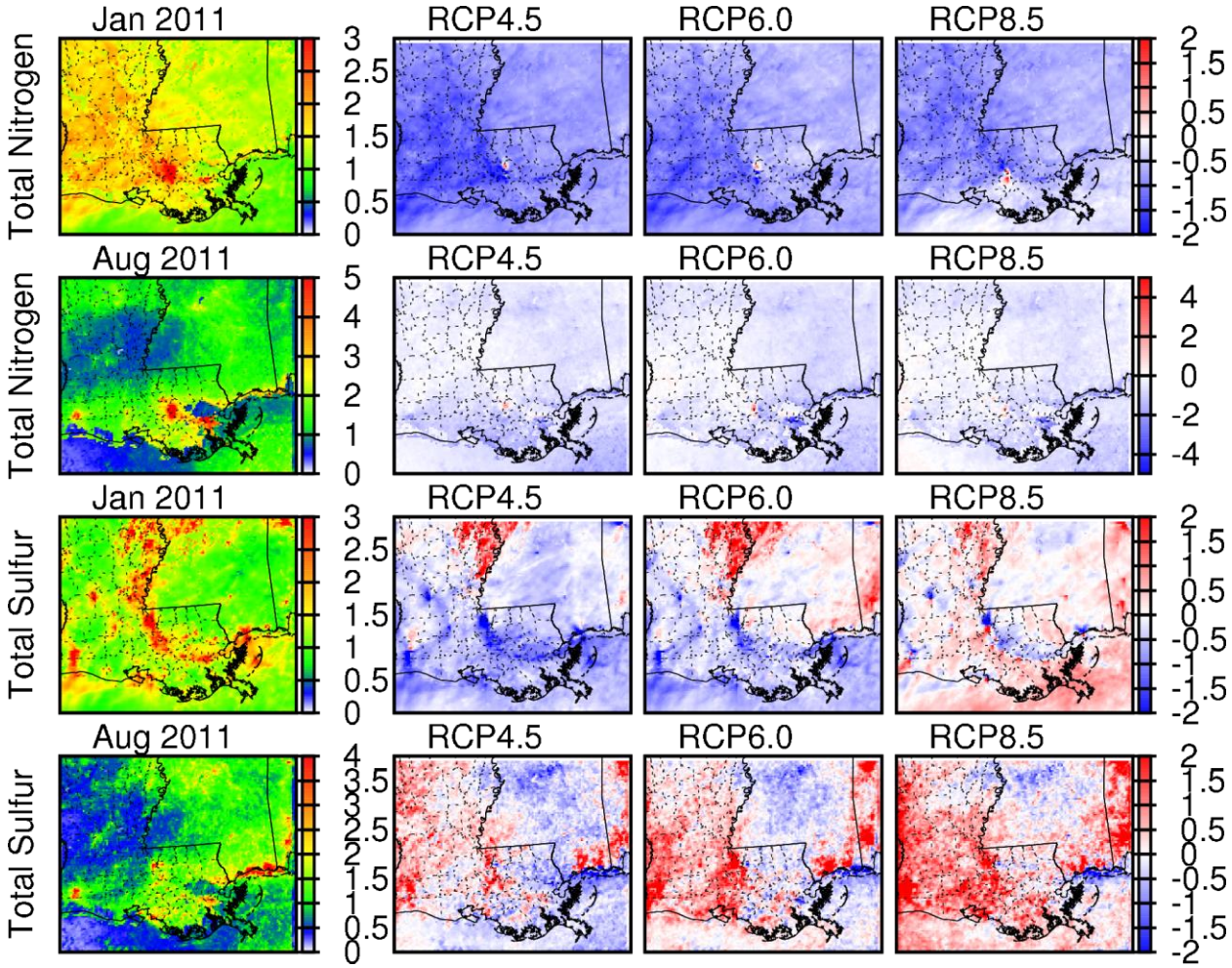

Figure 7. Total nitrogen and sulfur deposition fluxes in at Jan and Aug.2011 with the differences from 2050 to 2011 in RCP4.5/6.0/8.5 climate scenarios and controlled case of emission scenario (Unit: kg S/ha).

In conclusion, this study offers insights of nitrogen and sulfur deposition in future, and contributions of different sources. EGU, industry and upwind sources are major sources of sulfur deposition and on-road vehicles, industry, and other inexplicit sources are important to nitrogen deposition. No change case shows an increase trend in August 2050 with total nitrogen and sulfur deposition in all three climate scenarios, while BAU case shows a more significant increase in most part of Louisiana in both nitrogen and sulfur depositions in January and August 2050, but nitrogen depositions show a decreasing trend in January and August 2050 of RCP 4.5/6.0/8.5 climate scenarios in controlled case.

References

Bradley, B., Wilcove, D., Oppenheimer, M., 2010. Climate change increases risk of plant invasion in the Eastern United States. Biol Invasions 12, 1855-1872.

Byun, D., Schere, K.L., 2006. Review of the Governing Equations, Computational Algorithms, and Other Components of the Models-3 Community Multiscale Air Quality (CMAQ) Modeling System. Applied Mechanics Reviews 59, 51-77.

Skamarock, W.C., Klemp, J.B., Dudhia, J., Gill, D.O., Barker, D.M., Duda, M.G., Huang, X.-Y., Wang, W., Powers, J.G., 2008. A Description of the Advanced Research WRF Version 3. National Center for Atmospheric Research.

Tai, A.P.K., Mickley, L.J., Jacob, D.J., 2010. Correlations between fine particulate matter (PM2.5) and meteorological variables in the United States: Implications for the sensitivity of PM2.5 to climate change. Atmospheric Environment 44, 3976-3984.

Woo, J.-H., He, S., Tagaris, E., Liao, K.-J., Manomaiphiboon, K., Amar, P., Russell, A.G., 2008. Development of North American emission inventories for air quality modeling under climate change. Journal of the Air & Waste Management Association 58, 1483-1494.

Coupled chemical and hydraulic impacts of saltwater intrusion on the fate and transport of spilled chemicals in the Mississippi River

Basic Information

Title:	Coupled chemical and hydraulic impacts of saltwater intrusion on the fate and transport of spilled chemicals in the Mississippi River
Project Number:	2017LA114B
Start Date:	3/1/2017
End Date:	2/28/2018
Funding Source:	104B
Congressional District:	LA-06
Research Category:	Water Quality
Focus Categories:	Solute Transport, Water Quality, Geochemical Processes
Descriptors:	None
Principal Investigators:	Zimeng Wang

Publications

There are no publications.

Problem and Research Objectives

In the year of 2011, almost 10000 tons of 287 different chemicals spilled into natural water bodies in the U.S. from 1374 different facilities. The Mississippi River is one of the most important transportation waterways of the U.S. with very large chemical shipping fluxes very year. The Louisiana section of the Mississippi River connects the riverine and oceanic transportations. The complicated hydraulic conditions under the urban anthropogenic stress and the frequent natural water hazards in this region increase the risk of chemical spills in the riverine system.

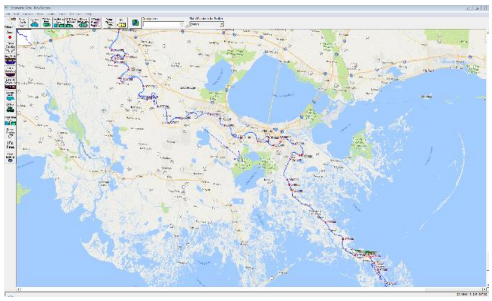

Figure 1. Mississippi River in South LA

MR is the trunk line of a massive natural transportation network that stretches as far northwest as Montana, and northeast to Pennsylvania. For instance, Port of Greater Baton Rouge is ranked as 8th in the US and is the furthest inland port on the MR that can accommodate ocean-going tankers and cargo carriers. Petrochemical production and manufacturing is a major industry in this state. Tons of crude oil and chemicals are transported on MR, many of which are hazardous materials with ecological and human health risks. This makes MR vulnerable to chemical spills due to the high mobility of the contaminants in advection flows and the risk to drinking water sources. This study investigated the 232 miles (371 km) of MR downstream of Baton Rouge to GOM which connects the riverine and oceanic transportations. It is treated as a long and narrow estuary (Figure 1).

The climate change cause sea level rise of the Gulf of Mexico and deteriorating inland drought has caused significant saltwater intrusion even in the flowing water of the MR. The complicated hydrological conditions under the urban anthropogenic stress and the frequent natural water hazards in this region increase the risk of chemical spills in the riverine system.

To access the fate and transport of the spilled chemicals, it is desirable to have a holistic understanding of the environmental chemistry and hydrology, as well as how they interact with each other. The creeping of the saltwater can retard the transport of spilled chemical through the river and also profoundly impact the solubility, volatility, partitioning and degradation of the chemicals. Experimental determination of the salinity effect on the chemical fates and modeling of hydrological processes of saltwater creeping inland can provide more precise evaluation of the contaminant migration and ecological impacts in the critical aquatic ecosystem in Southeast Louisiana.

Methodology

Hydraulic model of MR

HEC-RAS, the abbreviation of Hydrological Engineering Center (of USCOE) River Analysis System, was selected in this study. It is a free program and contains several river analysis components for: 1) steady flow water surface profile computations; 2) one- and two-dimensional unsteady flow simulation; 3) movable boundary sediment transport computations; and 4) water quality analysis. In particular, HEC-RAS simulates one-dimensional; two-dimensional; and combined one/two-dimensional unsteady flow through a full network of open channels, floodplains, and alluvial fans. The unsteady flow component can be used to performed subcritical, supercritical, and mixed flow regime (subcritical, supercritical, hydraulic jumps, and draw downs) calculations in the unsteady flow computations module. With regard to water quality simulation,

HEC-RAS incorporates advection-dispersion module which can model water temperature, dissolved nitrogen (NO_3-N, NO_2-N, NH_4-N, and Org-N); dissolved phosphorus (PO_4-P and Org-P); algae; dissolved oxygen (DO); and carbonaceous biological oxygen demand (CBOD). After comprehensive evaluation of a variety of computer program, HEC-RAS is considered as a good tool to accomplish the research objectives.

The investigated MR section is not a closed channel, instead it has a number of spillways and channels. Spillway is artificial water passage when water level in MR is higher than a set value. Channels are either natural or artificial passage where water leave MR. The artificial channels are constructed because coastal Louisiana is in danger of being washed away and inundated by GOM. Decades of river modifications, powerful hurricanes, resource extraction, and relative sea level rise have caused major coastal land losses. There needs to be adequate flow in the river to carry nutrient-rich sediment to the delta, overtop the natural levees, and combat saltwater intrusion from the GOM, to create additional land mass. These diversions remove a pre-designed percentage of the river's sediment-laden flow and direct it to specific areas in need of replenishment (McCorqupdale 2010). 2013 USAOE hydrographic survey book of MR was reviewed and used to create the river channel and cross section in HEC-RAS model. The major spillway, channels, and passes are included into the hydraulic analysis.

Hydraulics data in January 2018 were obtained from USGS gauge stations located along the MR. The water flow data were collected every 15 minutes. The data suggested the flow at MR at Baton Rouge ranged between 250,000 and 450,000 ft^3/s, and the average flow was 359,5000 ft^3/s (10,180 m^3/s) at this month. The average water travel time for water from Baton Rouge to GOM was estimated to be 7 days at this flow. So one month is adequate for simulating the river hydraulics. There is not gauge station at the mouth of GOM. The water level in the GOM was obtained from two USGS-maintained gauge stations located at GOM. The average water level at the mouth of MR is -0.055 feet, which was used as one of the boundary condition for the simulation.

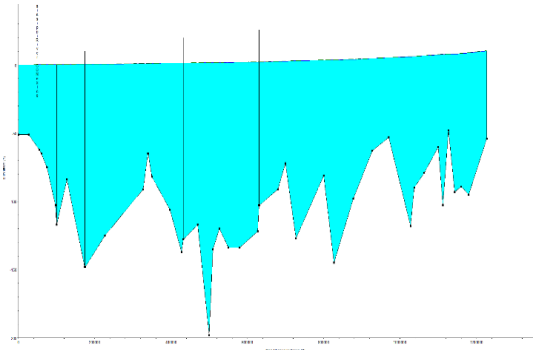

Figure 2. Riverbed Profile of the MR

Discharge records from the major passes indicate that up to 30% of the flow in the MR is lost between Bohemia (38.6 miles or 62 km north of GOM) and Baptiste Collette (11.5 miles, or 18 km north of GOM). All these passes are simulated as one pass in this study. The water flow profile is shown in Figure 2, where GOM is located at the left side and water flows from right to left. It shows the river bed is approximately 50 feet below NAVD88 at GOM; and the water bed is as deep as -60 m (-200 ft) above NAVD88 at 94 RM (150 km). The deepest point is at the French Quarter at the City of New Orleans (McCorquodale, 2010). The hydraulic model will be calibrated after obtaining more public data from USGS and US COE and more field sampling.

It is common sense that water flow velocities at each point at one specific cross section are not uniform. The water flow velocity close to the river bottom is zero (Figure 3). HEC-RAS has the capacity of dividing one specific cross section vertically into at most 45 slices and calculate their flow velocity respectively. As the flow in the river heads toward the Gulf of Mexico, it enters distributaries or passes. The amount of flow discharged into each pass is determined by the geometry of the passes, the energy differential between the upstream and downstream ends of the pass and to some extent the orientation of the pass with respect to the current in MR. Figure 4 shows the water flow velocity distribution at the Baton Rouge at the time zero of the simulation. The results suggest slice at deep water has the fastest flow speed of over 5.0 ft/s, while the shallow water has a velocity of as low as 1.0 ft/s. Therefore, the behavior of chemical spill occurring in the middle of the river will be different to the occurring at the shallow water. The disadvantage of HEC-RAS is that this program assume one cross section has uniform water quality results. In other words, this program assumes an instant and complete mixing occurs at the spill site.

Figure 3. water velocity distribution in a river. Longer arrow means higher velocity

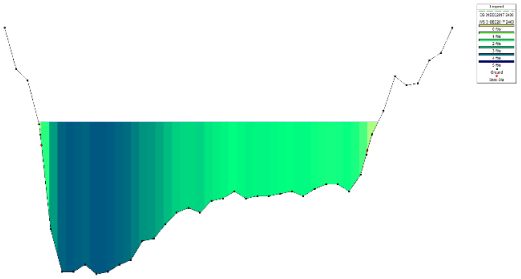

Figure 4. Water Flow Velocity Distribution in Cross Section

Dilution of Contaminants

For an instantaneous chemical spill occurring in a water body, the chemical concentration at one point (x, y, z) away from the emission point, at time t after the chemical spill is

$$C(x,y,z,t) = \frac{M}{4\pi t\sqrt{4\pi D_x D_y D_z t}} \exp\left(-\frac{x^2}{4D_x t} - \frac{y^2}{4D_y t} - \frac{z^2}{4D_z t}\right) \quad (1)$$

where M is the chemical mass; D_x, D_y, D_z are the diffusion coefficients in three directions. This equation works for any fluid materials such as air, water, or oil. If the water body is stagnant, the chemical spreads equally in all three directions as random Brownian Motion, mathematically described as a Gaussian distribution over time. The diffusion driving force is the concentration gradient. The molecular diffusion coefficient D_m depends on temperature, viscosity of the entraining fluid and mass of the particles. Molecular diffusion can also occur without an initial concentration gradient. In time the diffusion process will eventually result in complete mixing. D_m is small compared to other diffusion coefficients. For instance, D_m of ethanol in water is 8.4 X 10^{-10} m^2/s at 25 ^oC and 1 atm.

When the water moves in the water body, advection will enhance mass transfer. We can simplify a river to a channel with constant cross section area A and flow Q, the flow velocity at anywhere is Q/A. Water motion in this channel is therefore 1-D. The chemical concentration at x m downstream of emission point at time t is:

$$C(x,t) = \frac{M}{A\sqrt{4\pi Dt}} \exp\left(-\frac{(x-(x_0+ut))^2}{4Dt}\right) \quad (2)$$

where x_0 is the coordinate of the emission point. Eq. (2) suggested at the moment when the center of the spill hit the sampling point, the chemical spill has highest concentration at this point. When the sampling point is far from emission point, i.e, x-x_o>>ut, the chemical concentration at sampling point is virtually zero. When water velocity u is close to zero, Eq. (2) becomes Eq. (1). On the other hand when water moves at fast speed, the chemical will move as a strict plug flow. In other words, chemical can be detected at $t = (x-x_o)/u$, no chemical at other moment. When water moves at medium velocity, the temporal variation of chemical concentration at that point is Gaussian distribution.

Fast water motion also generates turbulence such as eddies which can cause random mixing, which is similar to Brownian motion but at a larger scale. A large diffusion coefficient termed as turbulent diffusion coefficient D_t is used to describe turbulent mixing. The largest eddies are usually limited by the smallest spatial dimension. That is depth in a river. This means that turbulent properties in a wide river is independent of the width, but dependent on the depth. Also, turbulence generates in zones of high shear, which is river bed. Baton Rouge section of MR is about 1,000 m wide, and the deepest point is only 25 m. Shear stress can be measured by shear velocity u*, which equals $\sqrt{ghS}$ for uniform open channel flow, where h is the depth of the river, g is the gravity acceleration and S is the channel slope (Socolofsky, 2005).

Most rivers have irregular cross sections, the depth of the river is then determined by the cross section area A and width of water surface W at one specific cross section area. The cross section area can be obtained by dividing the cross section into a few rectangular sections. For the MR at Baton Rouge, the depth h is calculated to be 18 m (60 ft). For the investigated river section, the average slope is 1.15 X 10^{-5} m/m, u* is calculated to be 0.045 m/s. Similar to D_m, D_t can be described as $D_{t,x}$, $D_{t,y}$, and $D_{t,z}$. $D_{t,z} = 0.067hu$*, The vertical turbulent diffusion coefficient for MR is 0.054 m^2/s. For a rectangular shape channel with same cross section area and uniform slope, $D_{t,y}$, i.e, transverse mixing shall be zero. In natural streams, the cross-section is rarely of uniform depth, and the fall-line tends to meander. These two effects enhance transverse mixing in natural streams. $D_{t,y} = 0.6hu$* (Tayfur 2005). For MR in Baton Rouge, $D_{t,y}$ is 0.49 m^2/s. $D_{t,x}$ is the same as $D_{t,y}$. So D_t is substantially higher than the D_m, D_m is therefore not considered in this study.

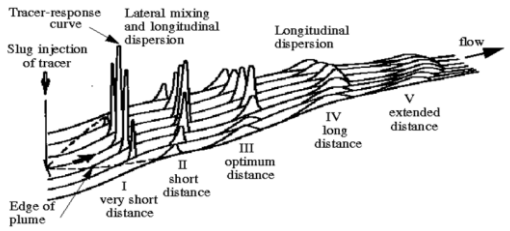

Figure 5. Lateral mixing and longitudinal dispersion patterns and changes in distribution of concentration downstream from a single, center, slug injection of tracer (Modified from Kilpatrick, 1993, p.2)

The water velocity in each point of one specific cross section is non-uniform as a result of the shear friction at the river bed and water internal friction (Figure 3). The shear-flow profiles in y and z directions will affect the transport of contaminants in natural stream. For an instantaneous injection of inert, soluble chemical into the river channel, the chemical will diffuse immediately in y and z directions. With the water moving forward, chemical also moves downstream in x direction. As shown in Figure 3, water move velocity in z direction is not uniform. At the river bed, the water velocity is virtually zero. Similarly, water flow velocity at the both banks is zero in y-direction. Therefore, the chemical spill become a 3-D plume moving downwards. Figure 5 shows the mass

transfer in a river. The shape of the plume is determined by the location of the emission point in three dimensions and river hydraulics. The velocity gradients in *y* and *z* directions enhance the chemical concentration gradients in these directions. The combined process of advection and y, z diffusion is termed as longitudinal dispersion D_L, which is calculated by:

$$D_L = 0.011\frac{U^2W^2}{d\sqrt{gdS}} \tag{3}$$

where U is the mean stream velocity; W is the stream width; d is the stream depth at one specific cross section. We calculate the dispersion coefficient of MR at Baton Rouge is 15.4 m^2/s. It is obvious D_L is much higher than D_t. For a narrow and long estuary, a simple 1-D river model that incorporates a longitudinal dispersion coefficient and a time-average seaward water velocity is adequate (Hemond, 2015).

For this emission, the vertical mix distance L_z is 12 times of the river depth, which is 216 m. The transverse mixing distance L_y is $W^2/3h$, which is 18,520 m. In detail, a spill of 1,000 kg of nonreactive, soluble chemical occurs at main channel at Baton Rouge. Using the MR hydraulics at this location, we simulated the spatial and temporal variation of the chemical concentration at MR. The Figure 6 shows the water concentration downstream at t = 50 seconds.

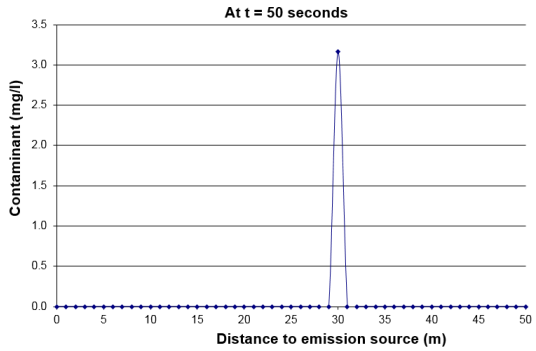

Figure 6. Pollutant Concentration at t =50 seconds

We investigated the scenario of instantaneous emission of nonreactive, soluble chemical at the water surface and 25% of the channel cross section. The plan and profile views of the river are shown in Figure 7. The chemical is released at point *A* at time T_0. With time goes on, the chemical diffuses in *x*, *y* and *z* directions. In *y* direction, the chemical diffuses systemically along around point *A*. At *x* direction, the chemical moves at different velocity as a function of how far they are away from the river centerline. In *z* direction, the chemical also diffuses because of concentration gradient.

Salt Water Intrusion

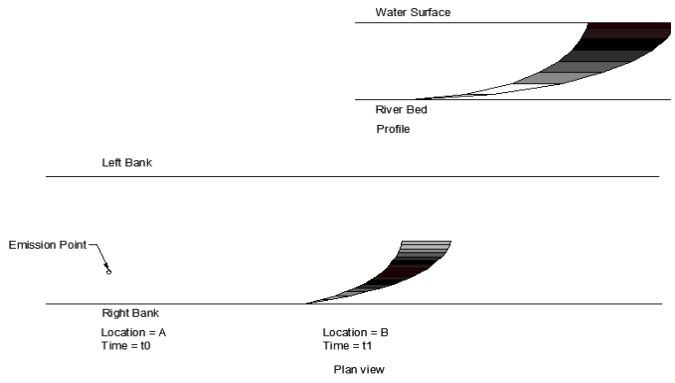

Figure 7. Simulation of chemical spill at 25% distance to right river bank

When a freshwater source such as a river enters a saltwater body, mixing between the two water sources creates brackish water. There are unique mixing processes involved in generation of the brackish water that occur at different spatial scales.

At the smallest scale, on the order of 10^{-11} m, diffusion occurs at the molecular level. Molecular diffusion process will eventually result in complete mixing as discussed before. At the largest scale, average flow brings two discrete bodies of differing salinity levels together to allow the intermediate scale of mixing to occur, also referred to as turbulence. In a stratified flow system, turbulent mixing occurs across the

interface of the two fluid bodies whereby salt is carried in the overlying fresh water by the mechanism of breaking internal waves, also referred to as Kelvin-Helmholtz instabilities. Turbulence along the interface greatly increases the surface area of the interface, allowing increased rates of molecular diffusion, which is the only mixing process that ultimately generates brackish water.

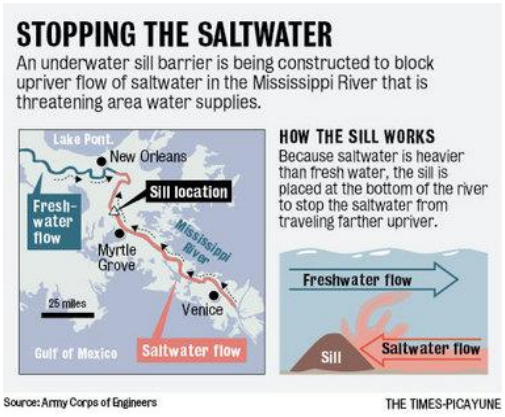

Figure 8. Salt Water Barrier in MR

Salt water encroachment impacts environment and economy in multiple aspects. One is the drinking water. City of New Orleans uses MR as major water source. A minimum of 300,000 ft^3/s (8,500 m^3/s) of fresh water passing New Orleans is required to keep the saltwater wedge from infiltrating the water supply intakes (LPBF, 2008). To solve this problem, ACOE dredged sediment to build up the barrier Myrtle Grove. The sill is located at 64 river miles north of GOM (Figure 8). Since completion of the 45-ft (13.7 m) channel, the sill has been constructed three times: in 1988, 1999, and 2012. The sill is currently approximately 9 m (30 ft) high. It is considered in this study.

With regard to chemical emission, stratification always inhibit the vertical transfer of dissolved chemicals from layer to layer. Rising salinity in water lowers the activity of dissolved ions due to higher ionic strength. Oxygen is less soluble in saline water than in fresh water; this may lead to fish kill in salty water layer in estuary.

After reviewing USGS and USAOE field data, the researchers selected specific conductivity (SC) as the indicator of salinity in MR. SC data of January 2018 were obtained in Baton Rouge and Golf of Mexico (Black Bay nr Stone Island nr Pointe-A-La-Hache). The average and maximum SC at Baton Rouge was 389 and 440 µs/cm respectively. In GOM, salinity was 27,589 µs/cm, 70 times higher than that of Baton Rouge. The SC of typical drinking water is within 50–500 µs/cm. The salinity in Baton Rouge is therefore acceptable for drinking purpose.

Salt water has a greater density (1.03 kg/L) than fresh water (1.00 kg/L). Salinity is more important than water temperature in water stratification in MR. In dry weather, when MR does not have sufficient freshwater, salt water moves upstream in the form of a wedge as shown in Figure 9. The one-dimensional, along-estuary salt conservation equation (Lerczak, 2006) is

$$A_o(x)\frac{\partial S_o}{\partial t} = \frac{\partial}{\partial x}\left[Q_f S_o + A_o(x)K(x)\frac{\partial S_o}{\partial x} \right] \tag{4}$$

where Q_f is the fresh water flow; S_o is the cross-sectional average salinity, and K is the along-estuary dispersion rate. This equation considers both concentration gradient and advection. When the rate of erosion of the saltwater along its leading edge is equal to the saltwater flow upstream along the channel bottom, the location of the wedge is stable, or "arrested". The maximum absolute distance of saltwater intrusion observed anywhere in the world occurred on the MR

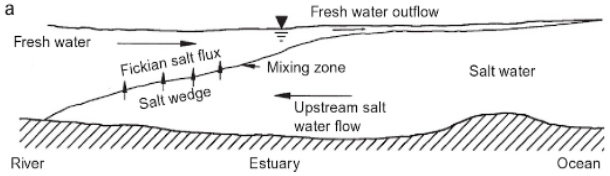

Figure 9. Salt Water Barrier in MR

in 1939 and 1940 when saltwater was observed about 225 km upstream from the mouth of Southwest Pass (Ayres 2015).

As shown in Figure 9, salt water will move vertically to fresh water layer in estuary in addition to move horizontally against fresh water. This is mainly due to salinity gradient and turbulent mixing, and temperature gradient to a less extent (MacDonald 2008). Vertical mixing is the most important process affecting the dynamics of estuaries as it determines the exchange flow, the stratification, residence time and distributions of waterborne material.

The stratification in estuaries is quantified by the buoyancy frequency $N = (g/\rho\ \partial\rho/\partial z)^{1/2}$ where ρ is the density of fluid to be measured. N is the angular frequency at which a vertically displaced water parcel will oscillate within a statically stable environment. The condition for stable stratification exists when $N^2 > 0$ and unstable stratification exists when $N^2 < 0$. High N suggests stratification is stable. N in estuary is much greater than in oceanic environments. Partially mixed estuaries have typical values of N of 0.05–0.1 s^{-1}, whereas salt wedge estuaries may have values of up to 0.3 s^{-1}. The back-and-forth movement of water driven by the ocean tide and river inflow enhances the dispersion and mixing along the freshwater-saltwater interface and mixed flows eventually reach the surface.

Turbulent flow is chaotic and random. In turbulent conditions, total shear stress between layers is mainly caused by eddies mixing, and by molecular diffusion to a less extent.

$$\tau = \mu\frac{\partial\bar{u}}{\partial z} - \rho\overline{u'w'} = \mu\frac{\partial\bar{u}}{\partial z} + \eta\frac{\partial\bar{u}}{\partial z} \tag{5}$$

In the above equation, μ is the viscosity of the water, u' is the turbulent velocity in the stream flow direction, w' is the turbulent vertical velocity; $\bar{u}$ is the average velocity; and η is the eddy viscosity. Turbulent mixing of salt and freshwater in estuaries affects the stratification, the length of the salinity intrusion, and the exchange of biological or chemical constituents between the river and coastal ocean. (Ralston 2010). Bottom boundary layer shear is the dominant source of turbulence and salinity mixing occurs primarily due to bottom boundary layer turbulence during flood tides.

The Reynolds-averaged Navier–Stokes equations (RANS) are primarily used to describe turbulent flows. Turbulent kinetic energy (TKE) is the mean kinetic energy per unit mass associated with eddies in turbulent flow. TKE can be produced by fluid shear, friction or buoyancy, or through external forcing at low-frequency eddy scales (integral scale). Physically, the TKE production is characterized by measured root-mean-square (RMS) velocity fluctuations $\overline{u_i'u_j'}$, also known as Reynolds stress as shown in Eq. (6). In the TKE production term, $\partial u/\partial z$ is the Reynolds-averaged vertical shear. It can be transported and dissipated. TKE transport includes diffusive and advective effects. TKE is dissipated by viscous forces at the Kolmogorov scale. The production, transport, and dissipation of TKE is governed by

$$\underbrace{\frac{\partial k}{\partial t}}_{\text{Local derivative}} + \underbrace{\bar{u}_j\frac{\partial k}{\partial x_j}}_{\text{Advection}} = \underbrace{-\frac{1}{\rho_o}\frac{\partial\overline{u_i'p'}}{\partial x_i}}_{\text{Pressure diffusion}} \underbrace{-\frac{1}{2}\frac{\partial\overline{u_j'u_j'u_i'}}{\partial x_i}}_{\substack{\text{Turbulent transport}\\ \mathcal{T}}} + \underbrace{\nu\frac{\partial^2 k}{\partial x_j^2}}_{\substack{\text{Molecular viscous transport}}} \underbrace{-\overline{u_i'u_j'}\frac{\partial\overline{u_i}}{\partial x_j}}_{\substack{\text{Production}\\ \mathcal{P}}} \underbrace{-\nu\frac{\overline{\partial u_i'}}{\partial x_j}\frac{\partial u_i'}{\partial x_j}}_{\substack{\text{Dissipation}\\ \varepsilon_k}} \underbrace{-\frac{g}{\rho_o}\overline{\rho' u_i'}\delta_{i3}}_{\substack{\text{Buoyancy flux}\\ b}} \tag{6}$$

The intensity of turbulence in estuaries is high compared with lake and the ocean. High stresses and high shear rates lead to high turbulent kinetic energy production (Geyer 2008).

A punctual and sustained source of buoyancy usually creates a continuous rise of lighter fluid through the ambient denser fluid, with mixing occurring along the way. Strong turbulence causes bigger buoyancy flux as shown in Equation 6. Because of the dominant influence of salinity on the density in these estuarine environments, the vertical buoyancy flux was almost entirely due to fluxes of salinity, with heat flux being a minor contributor. Buoyancy flux is also written as:

$$B = \frac{g}{\rho_0}\overline{\rho' w'} = -g\beta K_h \frac{\partial s}{\partial z} \tag{7}$$

where ρ_0 is the mean density; $\overline{\rho'}$ is the density fluctuation; K_h is the eddy diffusivity, an indicator of turbulence strength; β is the coefficient of saline contraction; $\partial s/\partial z$ is the salinity gradient in vertical direction (Wang, 2011). Estuary has both higher buoyancy frequency and turbulent dissipation rate than ocean environment. The dissipation rate was highest near the bottom, monotonically decreasing in vertical direction. This is easily understandable since estuary bottom has the highest velocity gradient.

Quantifying the parameters of TKE equation is necessary for studying the chemical transport in MR.

Principal Findings and Significance

In general, this study accomplished the following goals:

1) simulated the hydraulics of MR

2) established the theoretical framework of the simulating chemical fate and transport; and,

3) reviewed hydraulics characterizing the stratification and turbulence of MR and GOM.

Following conclusions are drawn based on the work performed:

- HEC-RAS is ideal tool for simulating the hydraulics of stream like MR. However, this program is not able to simulate the water quality distribution at one specific cross section.
- 2) HEC-RAS along is not able to simulate the stratification of salt water and fresh water. combining other program and algorithm is necessary.

Work in progress

In this study, we investigated the easiest spill, i.e., instantaneous release of nonreactive, soluble chemical at river surface. Real world spills are more complicated. Chemically, it can be biodegradable, such as chemical fertilizers; it can be soluble or insoluble in water; with regard to spill location, it can occur at river middle, or bank; vertically, it can emit at water surface or at a few meter below river surface; for release pattern, it can be instantaneous, or last a few hours even a few days.

As rule of thumb, rising salinity in water can lower the activity of dissolved ions and oxygen solubility. Considering petrochemical industry is important in south Louisiana, we will study the chemical behavior of typical chemicals such as benzene at varying conditions such as DO, salinity, or sediment contents. Publically available salinity data from USGS and USACOE are inadequate to support the research. So the researchers are planning to talk to USGS and US ACOE, City of New Orleans to undertaken some field measurement and sampling. To investigate the salinity distribution along the river course and vertically, we are planning to collect water sample at the following locations:

1) New Orleans French Quarter

2) Belle Chasse,

3) the river mouth of MR

The water samples will be collected at the water surface and deep in water at a few meters interval. We will measure specific conductivity, flow velocity, water temperature, density to determine the extent of mixing and stratification. The objective is to draw a spatial and temporal salinity distribution database in the MR between Baton Rouge and GOM.

Abbreviation and Explanation:

D_m: molecular diffusion coefficient (m^2/s)
GOM – Gulf of Mexico
MR: Mississippi River
N: buoyancy frequency
RM – River Mile. The distance from the connection point of Golf of Mexico and Mississippi River to the interest point along the river course.
S: Channel slope (m/m, or ft/ft)
SC-specific conductivity (us/cm)
u - velocity horizontal velocity in the stream-wise direction
w- velocity in vertical direction

References:

Ayres, S. University of New Orleans. *A Simulation of the Mississippi River Salt Wedge Estuary Using a Three-Dimensional Cartesian Z Coordinate Model*. Ph.D dissertation, 2015

Geyer, W., Scully, M. and Ralston, D. *Quantifying Vertical Mixing in Estuaries*. Environ Fluid Mechanics (2008) 8:495–509

Hemond, H., and Fechner, E. *Chemical Fate and Transport in the Environment*. 2015. Elsevier. 3rd edition.

Kilpatrick, F. *Simulation of soluble waste transport and buildup in surface waters using tracers.* Techniques of Water-Resources Investigations of the United States Geological Survey, Chapter A20. 1993

Lake Pontchartrain Basin Foundation (LPBF). (2008). *Comprehensive Recommendations Supporting the Use of the Multiple Lines of Defense Strategy to Sustain Coastal Louisiana 2008 Report (Version 1)*, Lake Pontchartrain Basin Foundation. Metairie, LA.

Leeuwen, V., and Hermens, J. *Risk Assessment of Chemicals: An Introduction.* Springer Science + Business Media. 1995.

Lerczak, J. and Geyer, W. *Mechanisms Driving the Time-Dependent Salt Flux in a Partially Stratified Estuary*. Journal of physical Oceanography. 36 (2006)

MacDonald, D. and Horner-Devine, A. *Temporal and Spatial Variability of Vertical Salt Flux in a Highly Stratified Estuary*. Journal of Geophysical Research 113 (2008)

McCorquodale, A., Georgiou, I., Davis, M., and Pereira, J. *Hydrology and hydrodynamic modeling of The Mississippi River in Southeast Louisiana*. 2010

Ralston, D., Geyer, W., Lerczak, J., and Scully, M. *Turbulent Mixing in a Strongly Forced Salt Wedge Estuary.* Journal of Geophysical Research 115 (2010)

Socolofsky, S., and Jirka, G. *Special Topics in Mixing and Transport Processes in the Environment. Engineering Lecture*. Texas Agricultural Machinery University. 2005. 5th edition.

Tayfur, G., and Singh, V. *Predicting Longitudinal Dispersion Coefficient in Natural Streams by Artificial Neural Network*. Journal of Hydraulic Engineering. 2005, 131(11):991:1000

Wang, B., Giddings S., Fringer, Gross, O., Fong, D. and Monismith, S. *Modeling and Understanding Turbulent Mixing in a Macrotidal Salt Wedge Estuary*. Journal of Geophysical Research 116 (2011)

Desalination of salt water for agriculture based on a novel battery system

Basic Information

Title:	Desalination of salt water for agriculture based on a novel battery system
Project Number:	2017LA115B
Start Date:	3/1/2017
End Date:	2/28/2018
Funding Source:	104B
Congressional District:	LA-06
Research Category:	Engineering
Focus Categories:	Water Quality, None, None
Descriptors:	None
Principal Investigators:	Xiuping Zhu

Publication

1. X.P. Zhu, W.W. Xu, G.C. Tan, Y. Wang. Concentration Flow Cells for Efficient Salinity Gradient Energy Recovery with Nanostructured Open Framework Hexacyanoferrate Electrodes. ChemistrySelect. 2018, DOI: 10.1002/slct.201800312.

Problem and Research Objectives

Salinity affects plant growth, resulting in lower crop yields and reduced agricultural production. As soil salinity increases, most plants are difficult to extract water from the soil. Increased levels of salt can also disturb the balance of plant nutrients in the soil and some salts are even toxic to certain plants. Salinity will also affect the physical and chemical properties of soil, resulting in surface soil compaction and erosion. High levels of salt can dehydrate soil bacteria and fungi and reduce soil health, which is depended on good microbial activity for the formation of organic matter and nutrient recycling. The breakdown in soil structure, together with the associated loss of plant cover, results in a greater exposure of the soil to erosion. Sheet, rill, gully and wind erosion is commonly caused by salinity.

The aim of this project is to develop a novel method (Figure 1) for saltwater desalination with low energy consumption based on NaCl salinity gradient (NaClSG) batteries.

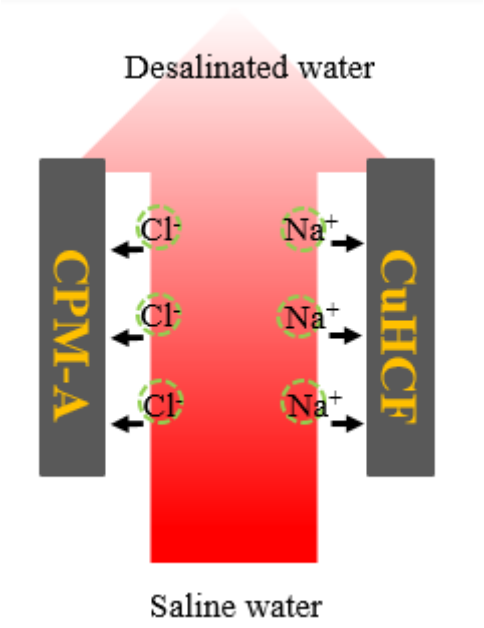

Fig. 1. Working principle for saltwater desalination

Methodology

1. Preparation of the electrode materials

Activated peat moss (designated CPM-A) was produced through the pyrolysis carbonization process. The compressed peat moss biomass was purchased from Premier Horticulture Company, Canada (20 kg in pack). Before the synthesis process, impurities (including small wood sticks, coarse stalks of peat moss, etc.) in the peat moss were thoroughly picked out, leaving only the fine peat moss leaves. For the pyrolysis carbonization process, nearly 10 g peat moss precursor is loaded in a tubular furnace and carbonized at 1000 °C with argon flow of 100 sccm min^{-1}. The heating rate is 5 min^{-1}. The obtained hard carbon is carefully washed in 20% KOH at 70 °C for 2

h and 2 M HCl at 60 °C for 15 h to remove the impurities. The purified samples are further rinsed by MQ-water and then collected by filtration. After drying at 120 °C for 12 h in a vacuum oven, carbonized peat moss (CPM) is achieved. The CPM specimens are further activated at 300 °C for 3 h (at a heating rate of 5 min^{-1} in the tubular furnace) in a dry air flow of 50 sccm min^{-1}. The obtained activated peat moss (CPM-A) is first ground and then washed with 2 M HCl and MQ-water again before use.

CuHCF powder was prepared by a co-precipitation method. Briefly, 2.90 g of $Cu(NO_3)_2 \cdot 5H_2O$ (Alfa Aesar, 98%) was dissolved in 120 mL deionized water and 1.97 g of $K_3Fe(CN)_6$ (Alfa Aesar, 99%) was dissolved in another 120 mL deionized water. Then, these two solutions above were simultaneously dropwise added into 60 mL deionized water with constant stirring. The final solution was kept for 6 hours. The tawny brown precipitate was collected by centrifugation, washed with deionized water for three times, and dried overnight in vacuum at room temperature.

To prepare electrodes, 70 mg corresponding powder, 20 mg carbon black (conductive carbon, Alfa Aesar, 99.5%), and 10 mg polyvinylidene fluoride (PVDF, Alfa Aesar) as binder were mixed in 0.5 mL dimethylformamide (Alfa Aesar, 99%) and ground by hand. A slurry containing this mixture was spread on both sides of carbon paper current collectors (4 cm × 4 cm) with a mass loading of ~5 mg/cm^2 and a working area of 3 cm × 3 cm (ca. 9 cm^2) in the middle. The electrodes were then dried overnight in vacuum at room temperature.

2. Construction and performance tests of NaClSG battery

NaClSG batteries were constructed with hexacyanoferrate electrode and activated peat moss electrode, and a fabric spacer in the middle. Short platinum wires were connected to each electrode as current leads. Two silicon gaskets (5 cm × 5 cm × 254 μm) provided circular water flow channels (area = 9 cm^2). Then, two thicker solid silicon gaskets (5 cm × 5 cm × 508 μm) and two end plates (5 cm × 5 cm × 3 mm) with an inlet and an outlet were added on both ends and firmly sealed using bolts and nuts.

The experiments were conducted in a continuously recycling system including a pump, a conductivity meter, a water tank and NaClSG battery. The analytical pure sodium chloride (NaCl) solution was employed as the target solution and the flow rate was 5 ml min^{-1}. Several current densities between 5 and 9 mA were used by a potentiostat (VMP3, BioLogic). The relationship between conductivity (mS cm^{-1}) and concentration (g L^{-1}) was obtained according to a calibration table made prior to the experiment. In each experiment, the conductivity variation of the NaCl solution was monitored and measured at the outlet using an ion conductivity meter.

The electrosorption capacity (mg g^{-1}) was defined as follows:

$$\text{Electrosorption capacity} = (C - C_0)V/M$$

where C and C_0 (g L^{-1}) represent the final and initial concentrations, respectively, V is the solution volume (L), and M is the total mass of the electrodes (g).

Principal Findings and Significance

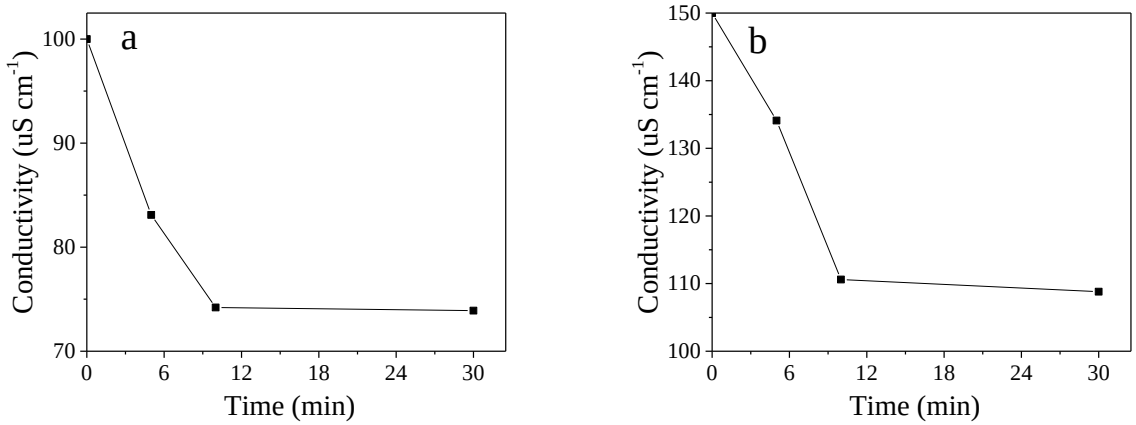

Fig. 2. Conductivity transient in different NaCl solution (a. 100 uS cm^{-1}, b. 150 uS cm^{-1}) at 9 mA.

During charging (the electric field is introduced on the electrodes), Na^+ and Cl^- can be attracted onto the surface of oppositely charged electrodes, which can be observed from the decrease of the solution conductivity. **Fig. 2(a)** shows the desalination behavior in NaCl solution with an initial conductivity of 100 uS cm^{-1}. **Fig. 2(b)** shows the desalination behavior in NaCl solution with an initial conductivity of 150 uS cm^{-1}. It is easy to observe that the desalination was very faster in the first ten minutes and became stable in the last twenty minutes, suggesting that the desalination rate is vey fast. Right now, the highest electrode desalination capacity was 9.27 mg-NaCl/g-electrode.

Information Transfer Program Introduction

None.

USGS Summer Intern Program

None.

Student Support					
Category	**Section 104 Base Grant**	**Section 104 NCGP Award**	**NIWR-USGS Internship**	**Supplemental Awards**	**Total**
Undergraduate	1	0	0	0	1
Masters	2	0	0	0	2
Ph.D.	9	0	0	0	9
Post-Doc.	1	0	0	0	1
Total	13	0	0	0	13

Notable Awards and Achievements

The LWRRI initiated a Louisiana Well Log Portal (https://sites.google.com/site/louisianawelllogportal/) in 2014. Up to date, more than 100,000 electric logs and drillers logs have been added to the Portal. This academic year more than 230 CEE undergraduate students were trained to analyze electrical logs and drillers' logs through course projects. Students learnt documenting well log data into Excel spreadsheets, making Google Earth kml files, and displacing well log data to Google Earth. The students' data were eventually deposited to the Portal after quality control. State agencies, the public, and private sectors have been using the Portal to understand Louisiana's geology and groundwater resources. The Portal has been visited by more than 5,600 times and more than 10 countries.

The LWRRI co-organized the 11th Annual Louisiana Groundwater, Surface Water and Water Resource Symposia, Louisiana State University, Baton Rouge, Louisiana, April 11-12, 2017

Publications from Prior Years

1. 2017LA-ADMIN ("") - Book Chapters - Pham, V.H., and F. T.-C. Tsai (2017), Chapter 48: Groundwater Modeling, Handbook of Applied Hydrology, edited by V.P. Singh. McGraw Hill.
2. 2017LA-ADMIN ("") - Articles in Refereed Scientific Journals - Pham, H.V., and F. T.-C. Tsai (2017), Modeling complex aquifer systems: a case study in Baton Rouge, Louisiana (USA). Hydrogeology Journal 25(3), 601-615. doi:10.1007/s10040-016-1532-6
3. 2017LA-ADMIN ("") - Articles in Refereed Scientific Journals - Mani, A., and F. T.-C. Tsai (2017), Ensemble averaging methods for quantifying uncertainty sources in modeling climate change impact on runoff projection. Journal of Hydrologic Engineering 22(4). doi:10.1061/(ASCE)HE.1943-5584.0001487
4. 2017LA-ADMIN ("") - Conference Proceedings - Pham, H.V., F. T.-C. Tsai, and K. Pohlmann. (2017), Grid generation and model calibration for complex fluvial aquifer system including geological faults, MODFLOW and More 2017, Golden, Colorado, May 21-24, 2017.
5. 2017LA-ADMIN ("") - Conference Proceedings - Tsai, F. T.-C., and A. Mani. (2017), Construction of Groundwater Systems with Very Large Well Log Dataset, World Environmental & Water Resources Congress 2017, Sacramento, CA, May 21-25, 2017
6. 2017LA-ADMIN ("") - Conference Proceedings - Tsai, F. T.-C., H.V. Pham and J. Yin. (2017), Quantifying Uncertainty Sources in Modeling Climate Change Impact on Runoffs, World Environmental & Water Resources Congress 2017, Sacramento, CA, May 21-25, 2017
7. 2017LA-ADMIN ("") - Other Publications - Yin, J. and F. T.-C. Tsai (2017). Saltwater Intrusion modeling for the Baton Rouge aquifer system, Southeast Louisiana, 11th Annual Louisiana Groundwater, Surface Water and Water Resources Symposium, Baton Rouge, Louisiana, April 11-12, 2017.
8. 2017LA-ADMIN ("") - Other Publications - Vahdat-Aboueshagh, H. and F. T.-C. Tsai (2017). A geological modeling framework based on well log data: A case study of Chicot Aquifer, southwest Louisiana, 11th Annual Louisiana Groundwater, Surface Water and Water Resources Symposium, Baton Rouge, Louisiana, April 11-12, 2017.
9. 2017LA-ADMIN ("") - Other Publications - Karakullukcu, R., D. Bhatta, F. T.-C. Tsai, and K. Paudel (2017). Construction of Mississippi River Alluvial Aquifer, Northeast Louisiana, 11th Annual Louisiana Groundwater, Surface Water and Water Resources Symposium, Baton Rouge, Louisiana, April 11-12, 2017.
10. 2017LA-ADMIN ("") - Other Publications - Li, A. and F. T.-C. Tsai (2017). Groundwater pumping induced land subsidence in the Baton Rouge area, Southeast Louisiana, 11th Annual Louisiana Groundwater, Surface Water and Water Resources Symposium, Baton Rouge, Louisiana, April 11-12, 2017.
11. 2017LA-ADMIN ("") - Other Publications - Tsai, F. T.-C., and A. Mani (2017). Conjunctive management of water resources for northern Louisiana under projected future climate change scenarios, 11th Annual Louisiana Groundwater, Surface Water and Water Resources Symposium, Baton Rouge, Louisiana, April 11-12, 2017.
12. 2017LA-ADMIN ("") - Conference Proceedings - Pham, H.V., F. T.-C. Tsai, and K. Pohlmann. (2017), Grid generation and model calibration for complex fluvial aquifer system including geological faults, MODFLOW and More 2017, Golden, Colorado, May 21-24, 2017.
13. 2017LA-ADMIN ("") - Conference Proceedings - Karakullukcu, R., F. T.-C. Tsai, D. Bhatta, K.P. Paudel, and S.-C. Kao, Development of a Mississippi River Alluvial Aquifer Groundwater Model, 2017 American Geophysical Union Meeting, December 11-15, (2017), New Orleans, Louisiana
14. 2017LA-ADMIN ("") - Conference Proceedings - Yin, J., and F. T.-C. Tsai, Impact of spatial pumping patterns on regional groundwater management: a case study to Baton Rouge aquifer system, southeastern Louisiana, 2017 American Geophysical Union Meeting, December 11-15, (2017), New Orleans, Louisiana

15. 2017LA-ADMIN ("") - Conference Proceedings - Li, A., F. T.-C. Tsai, N. H. Jafari, Q. J. Chen, and S. Bentley, (2017), A Geostatistical Toolset for Reconstructing Louisiana's Coastal Stratigraphy using Boring Data and Cone Penetrometer Tests, 2017 American Geophysical Union Meeting, December 11-15, 2017, New Orleans, Louisiana
16. 2017LA-ADMIN ("") - Conference Proceedings - Vahdat-Aboueshagh, H., F. T.-C. Tsai, D. Bhatta, K.P. Paudel, (2017), Toward developing more realistic groundwater models using big data, 2017 American Geophysical Union Meeting, December 11-15, 2017, New Orleans, Louisiana